Computational design of material-efficient steel truss bridges

Final report – Bachelor End Project

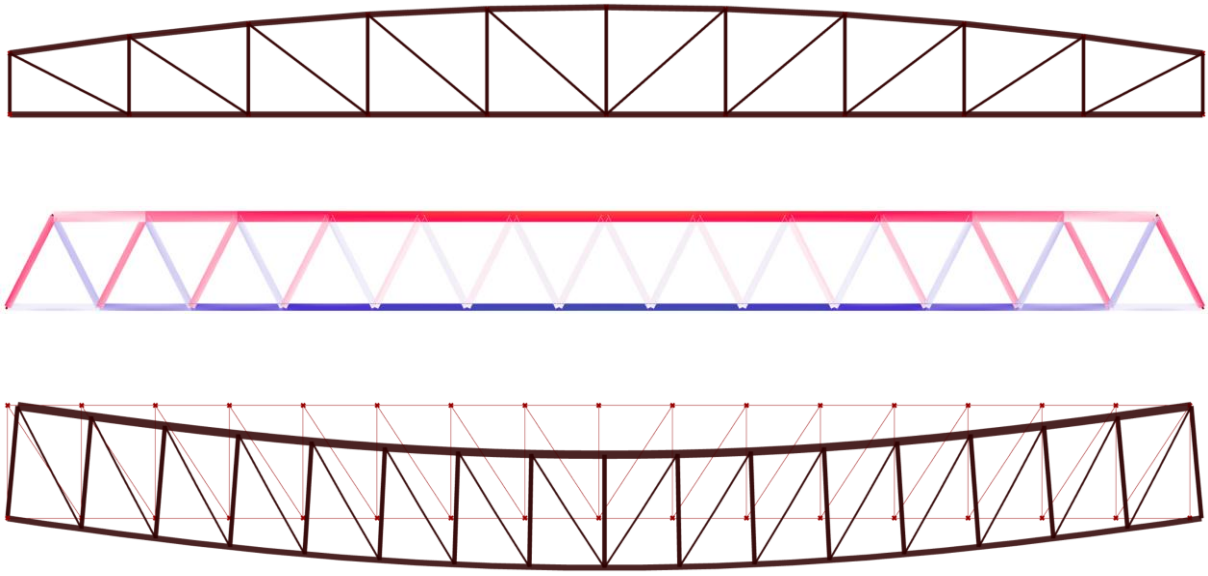

Author:
Wouter Kunst
5798027

Supervisors:
1st Supervisor: Dr. T. (Trayana) Tankova
2nd Supervisor: Dr.ir. P.C.J. (Pierre) Hoogenboom

Date:
19 June 2026

Delft University of Technology
Faculty of Civil Engineering and Geosciences (CEG)

TU Delft

Preface

This report is the result of my Bachelor End Project, which concludes my bachelor's degree. Over the past few months, I have worked on the parametric optimization of material-efficient steel truss bridges. It was a challenging project, but I learned a lot about combining structural engineering with computational design.

I want to thank my supervisors, Dr. T. Tankova and Dr.ir. P.C.J. Hoogenboom, for their help during this project. Their feedback and practical advice were very valuable in setting up the models and completing this research.

The content, models, and conclusions presented in this report are entirely my own work. The AI assistant Gemini was used strictly as a language and formatting tool to improve the readability, structure, and grammatical accuracy of the English text.

I hope you enjoy reading the report.

Wouter Kunst
Delft, 19 June 2026

Summary

In response to the growing demand for sustainable infrastructure and the high carbon footprint of steel production, this research investigates the material efficiency of steel pedestrian truss bridges using computational optimization. The objective is to identify how truss topology, span-to-height (L/H) ratios, and cross-sectional profiles influence the total structural mass for spans ranging from 20 to 60 meters.

A parametric model was developed using Grasshopper, Karamba3D, and the evolutionary solver Wallacei. This automated workflow systematically generated, evaluated, and optimized Pratt, Warren, and Parker truss topologies against strict Eurocode criteria for ultimate limit state (ULS) strength, member buckling, and serviceability limit state (SLS) deflection. In total, 18 distinct datasets were analyzed, comparing uniform open profiles (IPE, HEA, HEB) against hybrid configurations utilizing Circular Hollow Sections (CHS) for the web members.

The optimization results revealed three key findings. First, the algorithm actively prevents the traditional stiffness penalty by satisfying strict deflection limits through global geometric adjustments (L/H ratios) rather than increasing profile weights. For constant-height trusses, an L/H ratio of 1:13 to 1:16 proved optimal. For the Parker truss, a flatter midspan ratio of 1:10 to 1:13 was significantly more efficient than traditional deep-arch guidelines suggest for pedestrian loads.

Second, the structural superiority of the topologies is span-dependent. While the Warren truss is most efficient for shorter spans utilizing heavier cross-sections, the Parker truss consistently becomes the most material-efficient topology for any span exceeding 40 meters, regardless of the selected profile.

Finally, integrating buckling-resistant CHS profiles in the web members yielded massive material savings. Transitioning to a hybrid configuration reduced the total structural mass by up to 27.5% for the Warren topology. Ultimately, this research demonstrates that replacing traditional, iterative design methods with an integrated algorithmic workflow significantly minimizes material waste by perfectly tailoring geometry and profile selection to specific span and load conditions.

Table of Contents

1 Introduction 1
1.1 Context 1
1.2 Problem statement 1
1.3 Objective 1
1.4 Research questions 1
1.5 Scope 2
2 Literature review 3
2.1 Truss topologies 3
2.1.1 Pratt truss 3
2.1.2 Warren truss 3
2.1.3 Parker truss 4
2.1.4 Howe truss 4
2.2 Cross sections 5
2.2.1 Open I-profiles 5
2.2.2 Circular hollow sections 5
2.3 Span-to-height ratio 6
2.4 Algorithmic and parametric optimization of steel truss bridges 6
3 Methodology 7
3.1 Constraints and loads 7
3.1.1 Boundary conditions and structural constraints 7
3.1.2 Load cases and 2D idealization 7
3.1.3 Load combinations and safety factors 7
3.2 Parametric model 8
3.2.1 Geometric generation logic 8
3.2.2 Parabolic logic of the Parker truss 8
3.3 Optimization 9
3.3.1 Local cross-section optimization 9
3.3.2 Design of experiments and profile subsets 9
3.3.3 Global geometric optimization via Wallacei 10
3.3.4 Penalty 10
4 Model validation and verification 11
4.1 Proof of concept and structural behavior 11
4.2 Analytical model verification 12
4.2.1 Structural forces 12
4.2.2 Buckling verification 13

5 Results of the parametric optimization 14
5.1 Mass efficiency across span ranges (20-60m) 14
5.2 The impact of hybrid cross-sections 15
5.2.1 Warren truss optimization 15
5.2.2 Pratt truss optimization 16
5.2.3 Parker truss optimization 16
5.3 Span-to-height ratio 17
5.3.1 Pratt truss 17
5.3.2 Warren truss 17
5.3.3 Parker truss 17
5.4 Structural utilization versus vertical displacement 18
6 Discussion 19
6.1 Solving deflection through global geometry 19
6.2 Comparing the L/H ratios to literature 19
6.3 The mass reduction of hybrid cross-sections 20
6.4 Model limitations 20
6.4.1 Missing wind loads 20
6.4.2 Idealized joints and connections 20
7 Conclusion & recommendations 21
7.1 Conclusion 21
7.2 Recommendations 21
Appendix A: Full Grasshopper script 23
A.1 Global overview 23
A.2 Geometry Pratt 24
A.3 Geometry Warren 24
A.4 Geometry Parker 25
A.5 Variables & evolutionary solver 25
A.6 Loads 25
A.7 Cross section optimalisation 26
A.8 Penalty 26
A.9 Visualisation 27
Appendix B: Full optimization datasets for all truss topologies 28
B.1 Pratt 28
B.2 Warren 29
B.3 Parker 30
Appendix C: Additional mass efficiency data 31

Appendix D: Uniform versus hybrid configurations 32
D.1 Pratt 32
D.2 Warren 33
D.3 Parker 34
Appendix E: Span-to-height ratios for HEA and HEB 35
Appendix F: ULS versus SLS 36
F.1 IPE 36
F.2 HEA 37
F.3 HEB 38
References 39

1 Introduction

1.1 Context

In modern cities, there is a growing demand for pedestrian and bicycle bridges to support sustainable transport. At the same time, the construction industry is under heavy pressure to reduce its carbon footprint. Because steel production causes high CO2 emissions, minimizing material use while keeping structures safe is a major goal in civil engineering today.

Steel is the most popular material for pedestrian bridges because it is strong, light, and durable. To use less steel, engineers are moving away from traditional, slow design methods and towards parametric optimization. Within this context of sustainability, automated optimization is necessary to design efficient bridges.

1.2 Problem statement

Steel trusses are highly efficient structures, making them a preferred choice for applications such as pedestrian bridges. The structural efficiency of these bridges depends heavily on their geometric proportions (such as the span-to-height ratio) and the topology of the truss system. Traditionally, designing these bridges is an iterative and manual process, which is time intensive. By using computational design, this conceptual design phase can be automated and optimized to significantly reduce material usage while maintaining structural integrity.

1.3 Objective

The primary goal of this Bachelor End Project is to develop a parametric model in Grasshopper and Karamba3D that automatically generates, analyzes, and optimizes the conceptual design of a steel pedestrian truss bridge. The objective is to find the most material-efficient (lowest mass) configuration for a given span, while strictly adhering to structural constraints regarding deflection, stress, and basic buckling checks. The script will optimize the truss topology, the geometric proportions and the profiles of the elements. Based on the results of this script an analysis will be made to show the most efficient configurations for steel pedestrian truss bridges with spans ranging from 20 to 60 meters.

1.4 Research questions

To support the objective, literature research will be done. For the literature research the following research question has been formulated:

- What is the influence of truss topology and geometric proportions on the volumetric material efficiency of steel pedestrian bridges for spans ranging from 20 to 60 meters?

To answer this research question the following sub-questions have been formulated:

- How does the span-to-height ratio (L/H) influence the total steel volume required to satisfy both strength and stiffness requirements?
- How do Pratt, Warren, and Parker truss topologies perform in terms of volumetric material efficiency when optimized parametrically for spans between 20 and 60 meters?
- To what extent do Hollow Structural Sections (HSS) improve material efficiency compared to open profiles (I-beams) across the 20 to 60-meter span range, specifically when considering member buckling?

1.5 Scope

To make sure the project can be finished in the given timespan restrictions will be made.

The scope of the project will be static analysis (ULS, SLS), linear elasticity of the material and vertical loads of pedestrian bridges (NEN-EN 1991-2) and load combinations (NEN-EN 1990). The profiles of the elements will be limited to IPE-, HEA-, HEB- and CHS-profiles. For the truss topologies there will be looked at 2D Warren, Pratt and Parker trusses.

This research will not look into horizontal loads, vibrations, fatigue of welds, foundations, joints/connections and aesthetics.

2 Literature review

2.1 Truss topologies

2.1.1 Pratt truss

The Pratt truss consists of vertical members, diagonal members that slope downwards towards the middle of the truss, and parallel top and bottom chords (Figure 2.1). When a vertical uniformly distributed load acts on the bridge, the top chord is subjected to compression while the bottom chord is under tension. Within the internal members, the longer diagonal members carry tension, whereas the shorter vertical members undergo compression (Hibbeler, 2012). This layout is highly efficient, because directing compression forces into the shorter vertical members significantly increases their resistance to buckling due to the reduced effective buckling length. Furthermore, because the Pratt truss maintains a constant height and uniform angles for its diagonals, it is easier and more economical to fabricate and install compared to variable-height alternatives, such as the Parker truss (Barker & Puckett, 2013).



Figure 2.1: Geometry of the Pratt truss, characterized by its constant height, vertical compression members, and diagonal members oriented to primarily resist tension.

2.1.2 Warren truss

The basic Warren truss does not have vertical members, which saves a lot of weight (Figure 2.2). Instead the structure has diagonal members that alternate between tension and compression (Hibbeler, 2012). Because the diagonals can be subjected to compression, their profiles need to be big enough to resist buckling. A major advantage of the layout of the Warren truss is its simplicity. Having fewer members (no verticals) means there are fewer connection nodes, which makes the Warren truss relatively cheap and easy to build (Barker & Puckett, 2013). However, for heavy loads, extra vertical members can be added to support the top chord and prevent it from buckling.



Figure 2.2: Geometry of the Warren truss, illustrating the constant-height chords and the alternating diagonal web members that distribute tension and compression forces.

2.1.3 Parker truss

The Parker truss is characterized by a curved top chord that aligns with the bending moment curve for a more optimal force transfer (Mazurek et al., 2016). For large spans, the bending moments in a bridge are significant, and the arched design of a Parker truss can absorb these forces much more easily, allowing for smaller and lighter steel profiles (Mazurek et al., 2016). However, because the height of the truss varies, each diagonal member has a different angle and length (Figure 2.3). This means every connection node is unique, which significantly increases the fabrication and installation costs compared to constant-height trusses like the Pratt truss (Barker & Puckett, 2013). For small spans, however, creating this arched shape is unnecessary, as it makes the central diagonals excessively long and adds unnecessary weight to the bridge. Another key aspect of this geometry is that the diagonals become steeper toward the center. Even though the shear force is highest near the supports, the diagonals at the ends are less steep, which is less ideal for resisting maximum shear. However, when analyzing the forces with the method of sections, it becomes clear that this is fully compensated for by the inclined top chord, which carries a significant portion of the vertical shear force (Hibbeler, 2012).

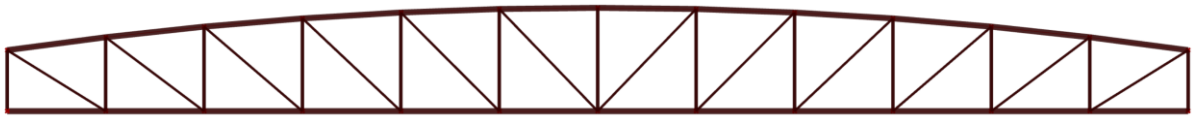

Figure 2.3: Geometry of the Parker truss, illustrating the characteristic curved top chord and the varying lengths and angles of the web members.

2.1.4 Howe truss

The Howe truss has parallel chords with diagonal members that slope upwards towards the middle of the truss (Figure 2.4). When a downward load acts on the bridge, the internal forces are reversed compared to a Pratt truss: the long diagonal members are under compression, while the shorter vertical members are under tension. In the 19th century, this design was highly popular. Builders back then frequently used wood for the diagonals because timber is good at resisting compression, and iron or steel for the vertical rods because it handles tension well. However, nowadays, the Howe truss is rarely used in steel bridge design. Because the longest members (the diagonals) are under compression, they are highly sensitive to buckling. Making these slender steel members strong enough requires very large and heavy profiles, which results in an inefficient use of material. It is far more efficient to have the longest members under tension, as seen in the Pratt truss (Nadimalla & Vanakudre, 2012). Because of this structural inefficiency, the Howe truss will not be considered for further analysis in this project.



Figure 2.4: The Howe truss configuration, illustrating the reverse diagonal orientation compared to the Pratt truss, which places the diagonal web members under compression.

2.2 Cross sections

2.2.1 Open I-profiles

Open I-profiles are characterized by asymmetric stiffness, as they are designed to optimally resist bending forces in a single direction about their strong axis (Figure 2.5). However, because the profile is open the flanges can move independently, which results in a very low torsional stiffness. Under bending loads, this low resistance to twisting makes open profiles susceptible to lateral torsional buckling, a phenomenon where the compression flange deforms laterally and twists (NEN-EN 1993-1-1). Open profiles offer major advantages for assembly and manufacturing. They allow for simple bolted connections using gusset plates because all surfaces are easily accessible from the outside. Furthermore, connecting these members does not require complex shapes, such as the saddle cuts needed for hollow sections, making workshop fabrication significantly cheaper and faster (Barker & Puckett, 2013).

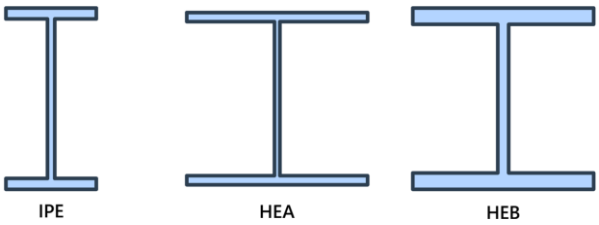

Figure 2.5: Cross-sectional geometry of IPE, HEA, and HEB profiles.

2.2.2 Circular hollow sections

Circular hollow sections (CHS) are characterized by a fully symmetrical cross-section, meaning the profile has no weak axis (Figure 2.6). This makes it the most structurally efficient profile for members subjected to compression, as it offers uniform resistance against buckling in all directions (NEN-EN 1993-1-1). Furthermore, because the profile is completely closed, the shear stresses caused by torsion can flow continuously in a circular path, resulting in an exceptionally high torsional stiffness. Despite these superior mechanical properties, circular hollow sections present significant challenges regarding fabrication and assembly. Creating welded connections is highly complex and expensive, as diagonal web members must be cut into intricate 3-D shapes, such as saddle cuts, to properly fit against the chords. Additionally, they are difficult to bolt because the closed nature of the profile prevents easy access to tighten nuts from the inside, requiring expensive specialized components or extra detailing if a bolted connection is preferred (Wardenier et al., 2010).

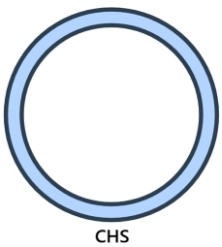

Figure 2.6: Cross-sectional geometry of a CHS profile.

2.3 Span-to-height ratio

An essential parameter in the conceptual design of a truss bridge is the span-to-height ratio (L/H), which has a big influence on the material efficiency and the structural stiffness of the truss. For parallel-chord systems, such as the Pratt and Warren truss, a uniform span-to-height ratio between 1:10 and 1:12 is standard to ensure sufficient vertical stiffness while minimizing total steel mass (National Steel Bridge Alliance (NSBA), 2025). When applied specifically to pedestrian bridges, where live loads are significantly lower than in highway or railway structures, this boundary can extend to a more slender ratio of approximately 1:14 (Roughan & O'Donovan Consulting Engineers, 2025).

For a variable-height system like the Parker truss, the structural height varies along the span, meaning its structural behavior must be captured using two distinct ratios (Roughan & O'Donovan Consulting Engineers, 2025). The midspan ratio (L/H_{mid}) typically ranges from 1:7 to 1:9 (Kumar & Kumar, 2018). The average height ratio ($L/H_{average}$) is often around 1:13 to 1:16 (Roughan & O'Donovan Consulting Engineers, 2025).

2.4 Algorithmic and parametric optimization of steel truss bridges

Recent academic literature in structural engineering highlights a significant shift toward automated, parametric workflows for optimizing steel truss structures. Traditional manual design iterations are increasingly replaced by integrated loops. Authors such as Kostić et al. (2024) show that coupling visual programming environments with Finite Element software (Karamba3D) allows for the efficient screening of hundreds of geometric variations to minimize steel volume. Yavan et al. (2024) further validate this shift, demonstrating how visual programming and evolutionary algorithms effectively bypass traditional trial-and-error limitations to systematically lower material consumption. Similar automated frameworks focused exclusively on self-weight reduction under strict structural criteria have been successfully implemented specifically for truss bridge geometries, utilizing genetic algorithms to drive cross-section efficiency (Li et al., 2023; Nguyen et al., 2024). This Bachelor End Project builds upon these established computational methodologies by applying them to a systematic comparative analysis of Pratt, Warren, and Parker topologies across a defined span range of 20 to 60 meters under Eurocode-compliant constraints.

3 Methodology

3.1 Constraints and loads

To evaluate the different truss topologies, a parametric calculation loop is established using Karamba3D. The system is analyzed at two levels: the Ultimate Limit State (ULS) for strength and stability, and the Serviceability Limit State (SLS) for deformation and user comfort.

3.1.1 Boundary conditions and structural constraints

The bridge is idealized as a two-dimensional (2D) model representing a single main truss girder. To ensure a statically determinate system and allow unconstrained thermal movement, the truss is configured with a hinged support at one end and a roller support at the other. For member buckling verification, Karamba3D determines the effective length of each element based on its actual centerline system length.

To satisfy the structural constraints, any geometry that violates the limits is systematically rejected by the algorithm. For the ULS, internal cross-sectional stresses must not exceed the 355 N/mm^2 yield strength of the utilized S355 structural steel. For the SLS, a strict vertical deflection limit of L/400 is implemented to ensure pedestrian comfort (Andersson & Hillberg, 2018).

3.1.2 Load cases and 2D idealization

The design incorporates permanent and variable load actions:

- **Permanent load (Self-weight):** Automatically computed by the finite element solver based on member cross-sections and a structural steel density of 78.5 kN/m^3.
- **Variable load (Pedestrian live load):** The uniformly distributed live load q_{fk} kN/m^2 is calculated as a function of the total span (L) according to NEN-EN 1991-2:2025:

$$q_{fk} = 2.0 + \frac{120}{L + 30}$$

Assuming a constant bridge deck width of 3 meters, the spatial load is shared equally between two parallel main girders. This total load is then converted into an equivalent 2D line load (kN/m) via Grasshopper and applied directly to the bottom chord:

$$q_{2D} = 0.5 \cdot 3 \cdot q_{fk}$$

3.1.3 Load combinations and safety factors

Load cases are calculated using the Karamba3D LoadCombination-component, applying the partial safety factors from fundamental combination equation 6.10b (NEN-EN 1990-1:2025+A1:2026):

- **ULS Combination:** The permanent self-weight is scaled by a factor of 1.35, and the variable pedestrian load by 1.5.
- **SLS Combination**: To verify the L/400 deflection criteria, a characteristic combination is applied with all load factors set to 1.0.

3.2 Parametric model

To systematically generate and analyze the Pratt, Warren, and Parker topologies across a range of structural variations, a flexible computational logic is established within the Grasshopper environment. The generation of each truss bridge configuration is governed by three primary input parameters controlled via numeric sliders: the total span (L) ranging from 20 to 60 meters, the maximum structural height (H) ranging from 1 to 10 meters, and the number of truss panels ranging from 5 to 25 panels. These input parameters serve as the initial boundary conditions that drive the automated generation of nodes and structural members. A complete visual overview and detailed sections of this parametric Grasshopper algorithm are provided in Appendix A.

3.2.1 Geometric generation logic

The script follows a standardized sequence to construct the mathematical layout of the constant-height Pratt and Warren trusses. First, the total span length is divided by the designated number of truss panels to determine the exact horizontal spacing and longitudinal coordinates of the bottom chord nodes along the global X-axis. This linear arrangement of points is subsequently duplicated and translated vertically along the global Z-axis according to the specified height parameter to establish the coordinates for the top chord nodes. When the positions of the nodes are defined, the structural elements are generated by drawing line segments that connect these points, automatically distinguishing between parallel chord elements, vertical web members, and inclined diagonals.

3.2.2 Parabolic logic of the Parker truss

While the Pratt and Warren configurations maintain a constant distance between the top and bottom chords, the Parker truss utilizes a variable height to align its geometry with the global bending moment distribution. To achieve this curvature, the vertical position of each node on the top chord is determined with a quadratic parabola equation. To constrain the parametric search space of the Parker truss within realistic engineering boundaries, the maximum height at midspan (H_{mid}) is bounded by a recommended span-to-height ratio of 1:7 to 1:9 (Barker & Puckett, 2013). The height at the supports (H_{start}) is mathematically driven to be roughly 50% to 60% of maximum height at midspan to ensure a structurally viable parabolic slope (Kulicki, 2014).

Using these boundary variables, the vertical coordinate h(x) of each individual top chord node is computed as a function of its specific horizontal coordinate x along the total span L using the following relationship:

$$h(x) = H_{start} + 4 \cdot (H_{mid} - H_{start}) \cdot \frac{x}{L} \cdot \left(1 - \frac{x}{L}\right)$$

This mathematical approach allows the computational script to automatically generate an optimized, tapered truss profile. In the central panels where the bending moment peaks, the equation increases the structural height, whereas near the supports where the bending forces approach zero, the geometry naturally tapers down.

3.3 Optimization

To construct the most material-efficient bridge topologies, a two-stage optimization workflow is implemented. This workflow combines local member sizing with global geometric form-finding.

3.3.1 Local cross-section optimization

Individual element capacity is optimized via the Optimize Cross Section (OptiCroSec) component in Karamba3D. This component iteratively evaluates a predefined catalog of standardized steel profiles against Eurocode 3 (NEN-EN 1993-1-1) criteria for cross-sectional resistance and member buckling. To maintain a constructible layout, members are grouped into distinct subsets, such as chords and web diagonals. The component analyzes the internal forces within each group and automatically assigns the lightest profile that satisfies the worst-case structural demands across that entire subset.

3.3.2 Design of experiments and profile subsets

To comprehensively evaluate the structural efficiency of different profile types, the optimization workflow was executed across 18 distinct datasets. For each of the three fundamental topologies (Pratt, Warren, and Parker), six specific cross-section combinations were investigated. These combinations were divided into uniform configurations and hybrid configurations:

Uniform configurations:

- **Dataset 1:** All structural members (chords and webs) restricted to IPE profiles.
- **Dataset 2:** All structural members restricted to HEA profiles.
- **Dataset 3:** All structural members restricted to HEB profiles.

Hybrid configurations:

- **Dataset 4:** Top and bottom chords restricted to IPE, with all web elements (diagonals and/or verticals) defined as CHS (Circular Hollow Sections).
- **Dataset 5:** Chords restricted to HEA, web elements defined as CHS.
- **Dataset 6:** Chords restricted to HEB, web elements defined as CHS.

This systematic categorization allows for a detailed comparative analysis between traditional open-section trusses and hybrid structural systems, specifically isolating the weight-saving potential of buckling-resistant CHS profiles in the web elements.

3.3.3 Global geometric optimization via Wallacei

To find the most material-efficient configuration, an automated optimization workflow is implemented by coupling Karamba3D with the evolutionary solver Wallacei. Mimicking the process of natural biological selection, the algorithm systematically searches for the optimal design by evaluating generations and applying mathematical crossover and mutation to the best-performing traits. The algorithm systematically manipulates the independent geometric variables: the span (L), the structural height (H) and the total number of truss panels (and specifically for the Parker truss, the midspan and support heights).

For each generated geometric variation, the local cross-section optimizer automatically selects the most efficient profile sizes from a predefined catalog, strictly adhering to Eurocode 3 (NEN-EN 1993-1-1) criteria. Configurations that violate the structural ULS or SLS constraints receive a severe penalty and are discarded from the genetic pool. The total structural mass of the surviving, valid configurations is subsequently fed back into Wallacei as the primary fitness function. This enables the evolutionary solver to systematically evaluate the design space and converge toward the global optimum across a span range of 20 to 60 meters, without violating any of the structural strength or serviceability constraints.

For each structural configuration, the evolutionary algorithm was configured with a generation size of 60 and a generation count of 100, resulting in 6,000 structural evaluations per run. Across all 18 datasets, the solver executed a total of 108,000 automated simulations to guarantee convergence toward the global optimum.

3.3.4 Penalty

To ensure that the evolutionary optimization algorithm strictly respects the structural boundary conditions, a heuristic penalty function has been implemented.

Following each iteration, the script verifies whether the actual stresses and displacements remain within the maximum allowable limits defined by Eurocode 3. If a design violates any of these ultimate limit state (ULS) or serviceability limit state (SLS) criteria, a penalty mass of 1 million kg is added to the true structural mass. Mathematically, the objective function is formulated as follows:

$$M_{\text{total}} = M_{\text{structure}} + M_{\text{penalty}}$$

where M_{penalty} is 1,000,000 kg if any structural constraint is violated, and 0 if the design is compliant. This massive inflation severely distorts the fitness landscape within Wallacei. By rendering non-compliant phenotypes highly unfavorable, the algorithm is forced to immediately discard unsafe configurations and converge exclusively toward structurally valid, optimized solutions.

4 Model validation and verification

4.1 Proof of concept and structural behavior

To validate the computational workflow and ensure the integrity of the parametric model, a preliminary analysis was conducted on a baseline truss configuration. This step serves as a proof of concept, demonstrating that the parametric geometry generated in Grasshopper is correctly interpreted by the Karamba3D finite element solver and that the structural system responds predictably to applied forces.

A preliminary simulation was executed using a standard constant-height Warren truss with a span of 20 meters. The model was evaluated under the simultaneous action of its permanent self-weight and the calculated pedestrian live load applied directly to the bottom chord elements. The initial analysis indicates that the model reacts in strict accordance with established structural mechanics:

- **Deformation and displacement:** Under the vertical downward loads, the truss exhibits a continuous, smooth parabolic deflection curve (Figure 4.1). The maximum vertical displacement is observed at midspan, which aligns perfectly with theoretical expectations for a simply supported beam system.

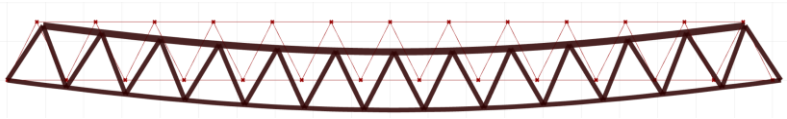

Figure 4.1: Displacement of the Warren truss under design loads (displacement scale exaggerated for clarity).

- **Internal force distribution:** The normal stress distribution matches the classic behavior of a Warren truss layout. The top chord is subjected to uniform compression (red), whereas the bottom chord experiences tensile forces (blue), with both forces peaking at midspan. Within the web elements the diagonals alternate between tension and compression. (Figure 4.2)

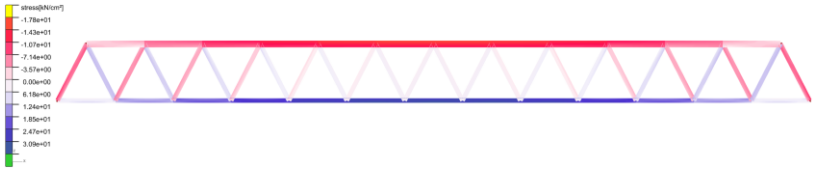

Figure 4.2: Normal stress distribution of the Warren truss under design loads, where blue indicates tension and red indicates compression.

The successful execution of this simulation confirms that the geometric logic, the load application, and the boundary supports are correctly mapped within the script.

4.2 Analytical model verification

Now that the baseline structural behavior is confirmed, the computational accuracy of the finite element solver is analytically verified. For the verification of the Grasshopper script a Warren truss with a span of 40 meters is evaluated. From the Wallacei solver the following optimal parameters were extracted: H = 2.4 m, number of panels = 13, L = 40 m and the structural mass = 4368 kg (Figure B. 3, Appendix B).

4.2.1 Structural forces

For the loads the ULS load combination has been used. To determine the permanent dead load, the total mass from Wallacei has been divided by the span and converted into an equivalent uniform line load acting on the bottom chord.

For the verification, the global bending moment and the theoretical normal forces in the top and bottom chords have been calculated using the following equations:

$$M_{max} = \frac{1}{8} \cdot q_{2D} \cdot L^2$$
$$N = \frac{M_{max}}{H}$$

For the normal force in the diagonals the following equations have been used:

$$V_{max} = 0.5 \cdot q_{2D} \cdot L$$
$$N = \frac{V_{max}}{\sin \theta}$$

where θ is the angle of the diagonal. The results of these manual calculations are compared to the computational Karamba3D outputs in Table 4.1.

Table 4.1: Comparison of computational (Karamba3D) and analytical (manual calculation) axial forces (N_{Ed}) for key structural members.

	Karamba3D (N_{Ed}) (kN)	**Manual calculation (kN)**	**Difference (%)**
Top chord (middle)	-846	-817	3.32
Bottom chord (middle)	+846	+817	3.32
Diagonal (support)	-220	-233	5.57
Diagonal (middle)	-1.1	0	-

The minor differences observed (< 6%) are due to the simplification of the dead load. In the manual calculation the total structural mass was converted into an equivalent uniform line load acting on the bottom chord. Karamba3D applies the self weight to each individual element based on its spatial location, distributing the load across both the top and bottom chords.

4.2.2 Buckling verification

For the buckling verification the most heavily loaded element in the middle of the top chord and the diagonal at the support are checked. The top chord is assigned an IPE330 profile, and the diagonal an IPE200 profile. The buckling check is performed according to the Eurocode 3 (NEN-EN 1993-1-1) criteria using the following equations:

$$N_{cr} = \frac{\pi^2 \cdot E \cdot I_z}{L_{cr}^2}$$

$$\bar{\lambda} = \sqrt{\frac{A \cdot f_y}{N_{cr}}}$$

$$\Phi = 0.5 \cdot \left[1 + \alpha \cdot \left(\bar{\lambda} - 0.2\right) + \bar{\lambda}^2\right]$$

$$\chi = \frac{1}{\Phi + \sqrt{\Phi^2 - \bar{\lambda}^2}}$$

$$N_{b,Rd} = \frac{\chi \cdot A \cdot f_y}{\gamma_{M1}}$$

$$Utilization = \frac{N_{Ed}}{N_{b,Rd}}$$

Table 4.2: Comparison of the analytical and computational buckling utilization for the top chord and diagonal.

	N_{cr} (kN)	λ	Φ	χ	$N_{b,Rd}$ (kN)	N_{Ed} (kN)	Manual calculation Utilization (%)	Karamba3D Utilization (%)	Difference (%)
Top chord	1725	1.135	1.303	0.514	1038	-846	81.5	81	0.61
Diagonal	363	1.669	2.142	0.287	264	-220	83.3	83	0.36

As demonstrated in Table 4.2, the difference between the analytical manual calculation and the computational utilization from Karamba3D is extremely small (< 1%). This minimal deviation indicates a highly accurate simulation and thereby fully validates the computational model for the automated optimization runs.

5 Results of the parametric optimization

5.1 Mass efficiency across span ranges (20-60m)

In this section, the pure mass efficiency of the Pratt, Warren, and Parker topologies is evaluated across a span range of 20 to 60 meters. To accurately isolate the influence of the global geometry, this initial comparison focuses exclusively on the uniform datasets, where all structural members are restricted to the same profile type (IPE, HEA, HEB).

While the main text focuses on the global mass trends and structural behavior, the complete dataset containing the exact optimized cross-sectional profiles and geometric variables for all 18 configurations across the 20 to 60-meter span range is documented in Appendix B.

As illustrated in Figure 5.1 (Dataset 1 - IPE), the Parker truss demonstrates superior material efficiency across the entire span range. When utilizing slender open profiles like IPE, the Warren truss is notably the heaviest configuration.

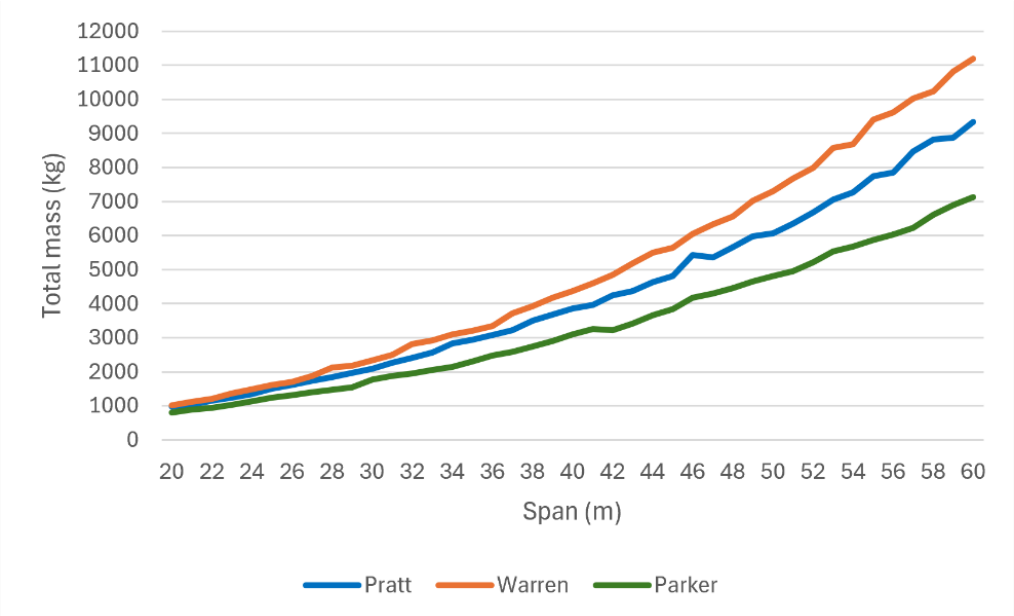

Figure 5.1: Total structural mass of the Pratt, Warren, and Parker topologies across a 20 to 60-meter span, utilizing uniform IPE cross-sections (Dataset 1).

However, a significant shift in structural efficiency is observed when the cross-sections are restricted to less slender profiles. While the Parker truss demonstrates superior material efficiency across the entire span range for IPE profiles, this superiority shifts for heavier sections. As depicted for HEB profiles in Figure 5.2 (and supported by the HEA dataset in Figure C. 1, Appendix C), the Warren truss initially outperforms the Parker topology for shorter spans.



Figure 5.2: Total structural mass of the Pratt, Warren, and Parker topologies across a 20 to 60-meter span, utilizing uniform HEB cross-sections (Dataset 3).

The Parker truss eventually surpasses the Warren configuration at a span of approximately 35 meters for HEA profiles, and at roughly 40 meters for HEB profiles. Despite these variations at shorter spans, a definitive universal trend emerges: for any span exceeding 40 meters, the Parker truss consistently proves to be the most material-efficient topology, regardless of the applied uniform profile.

5.2 The impact of hybrid cross-sections

This section highlights the structural efficiency gains when transitioning from uniform to hybrid cross-sections. While the main text illustrates this primarily using the IPE datasets, the complete set of mass comparison graphs for all profile combinations (IPE, HEA, and HEB) is documented in Appendix D.

5.2.1 Warren truss optimization

The optimization results for the Warren truss, presented in Figure 5.3, demonstrate the most significant structural efficiency gains among the three topologies. Due to the absence of vertical members, the diagonal web elements are forced to carry substantial compressive forces over long lengths, making them highly susceptible to buckling. Replacing these elements with buckling-resistant CHS profiles leads to a substantial efficiency improvement. At the maximum span of 60 meters, the hybrid configuration achieves a mass reduction of 27.5%, highlighting the critical role of cross-sectional shape in Warren-type systems (Table 5.1).

Table 5.1: Mass reduction of the Warren truss at key spans.

Span (m)	Mass Warren IPE	Mass Warren IPE CHS	Reduction (kg)	Reduction (%)
20	1012	771	241	23.8
30	2331	1750	581	24.9
40	4368	3270	1098	25.1
50	7296	6037	1259	17.3
60	11185	8110	3075	27.5

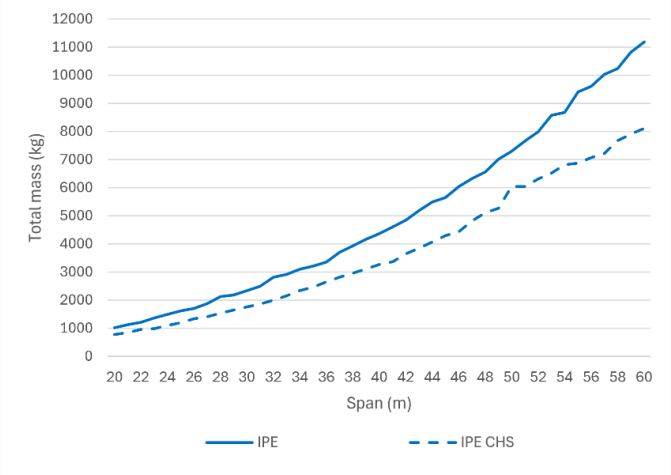

Figure 5.3: Total mass of the uniform IPE versus the hybrid IPE CHS configuration for the Warren truss.

5.2.2 Pratt truss optimization

As shown in Table 5.2 for the IPE configuration, the Pratt truss displays a moderate material reduction when transitioning from uniform open profiles to the hybrid configuration. Because the short vertical web members are primarily subjected to compression, their sensitivity to buckling is limited, which results in a consistent weight saving across the 20 to 60-meter span range. At a 60-meter span, the integration of CHS web members yields a mass reduction of 21.3% compared to the uniform IPE configuration (see Figure D. 1 in Appendix D for the detailed performance graph).

Table 5.2: Mass reduction of the Pratt truss at key spans.

Span (m)	Mass Pratt IPE	Mass Pratt IPE CHS	Reduction (kg)	Reduction (%)
20	974	756	218	22.4
30	2093	1672	421	20.1
40	3852	3128	724	18.8
50	6071	5120	951	15.7
60	9331	7339	1992	21.3

5.2.3 Parker truss optimization

While the parabolic geometry naturally optimizes force distribution and relieves the diagonal members, the inclusion of CHS web members provides a further refinement. As the span increases towards 60 meters, the buckling resistance provided by the circular hollow sections allows for an additional mass reduction of 12.3% (Table 5.3). While the relative savings are lower than in the constant-height trusses, it confirms that CHS profiles effectively complement the Parker's tapered geometry. The detailed performance graph illustrating this mass reduction is documented in Figure D. 7 in Appendix D.

Table 5.3: Mass reduction of the Parker truss at key spans.

Span (m)	Mass Parker IPE	Mass Parker IPE CHS	Reduction (kg)	Reduction (%)
20	794	641	153	19.3
30	1770	1463	307	17.3
40	3103	2580	523	16.9
50	4805	4076	729	15.2
60	7119	6241	878	12.3

5.3 Span-to-height ratio

For clarity and conciseness, the geometric analysis regarding the span-to-height ratio focuses exclusively on the IPE datasets. Preliminary review of the HEA and HEB datasets yielded comparable optimal geometric proportions (see Appendix E), indicating that the global L/H ratio is primarily driven by span length and deflection limits rather than the specific cross-sectional profile.

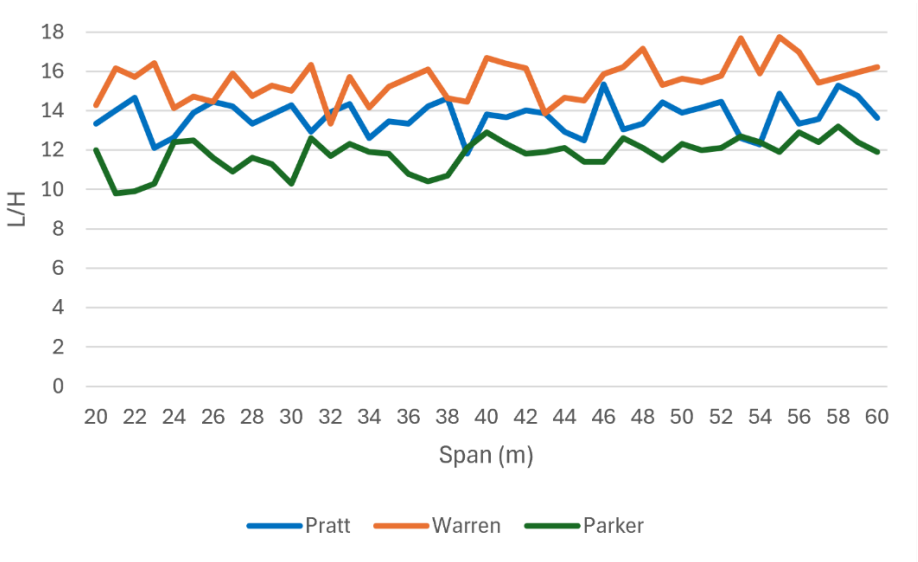

Figure 5.4: Optimal span-to-height (L/H) ratios for the Pratt, Warren and Parker topologies across the 20 to 60-meter span range, based on the IPE datasets.

5.3.1 Pratt truss

As illustrated in Figure 5.4, the computational optimization for the Pratt topology predominantly selected L/H ratios ranging between 13.0 and 14.5. This aligns perfectly with the standard theoretical upper boundary of 1:14 for pedestrian bridges. The algorithm consistently favors a relatively slender truss to minimize total steel mass, as the vertical members effectively handle compression without requiring excessive profile dimensions.

5.3.2 Warren truss

Interestingly, the optimization behavior for the Warren truss deviates slightly from the Pratt configuration (Figure 5.4). The algorithm selects noticeably more slender proportions, with ratios typically ranging from 14.0 to 16.5, slightly increasing as the span extends. This computational preference is a direct mechanical response to member buckling: by keeping the structural height relatively low, the length of the compression diagonals is minimized, thereby limiting their sensitivity to buckling and avoiding the need for excessively heavy cross-sections.

5.3.3 Parker truss

Due to its parabolic top chord, the span-to-height ratio for the Parker truss is evaluated at midspan (L/H_{mid}). While the literature (Kumar & Kumar, 2018) recommends L/H_{mid} ratios of 1:7 to 1:9, the evolutionary solver identified that for pedestrian bridges, the most material-efficient geometries are significantly flatter. The optimization predominantly selected midspan ratios between 9.8 and 13.2 (Figure 5.4). This demonstrates that for pedestrian applications, forcing a deep parabolic arch is inefficient. A flatter profile sufficiently resists the bending moments while avoiding excessively long internal web members.

5.4 Structural utilization versus vertical displacement

To evaluate which structural constraint governs the algorithmic design, the cross-sectional utilization (ULS) was plotted against the vertical displacement factor (SLS) for all optimized topologies. The Y-axis represents the ratio of the applied load or displacement relative to the maximum allowable limit, where 1.0 equals 100% capacity.

As illustrated in the performance tracking graph for the Pratt topology (Figure 5.5), a consistent and highly coupled behavior emerges across the 20 to 60-meter span range for the IPE datasets. Both the ULS utilization factor and the SLS displacement factor remain high, generally fluctuating between 0.85 and 1.0.

Even at the maximum span of 60 meters, where deflection typically becomes a critical governing factor, the data shows that the stress utilization of the structural elements does not experience a significant drop. The optimization model achieves a state where the structural components are operating near their maximum allowable limits for both strength and stiffness simultaneously, across all evaluated spans. This coupled structural behavior is similarly observed across the Warren and Parker topologies.

However, data for the heavier HEA and HEB profiles show a lower SLS factor at shorter spans due to their natural cross-sectional stiffness, eventually converging towards 1.0 at larger spans. The complete set of ULS/SLS performance tracking graphs for the Warren and Parker topologies, as well as all HEA and HEB configurations, is documented in Appendix F.

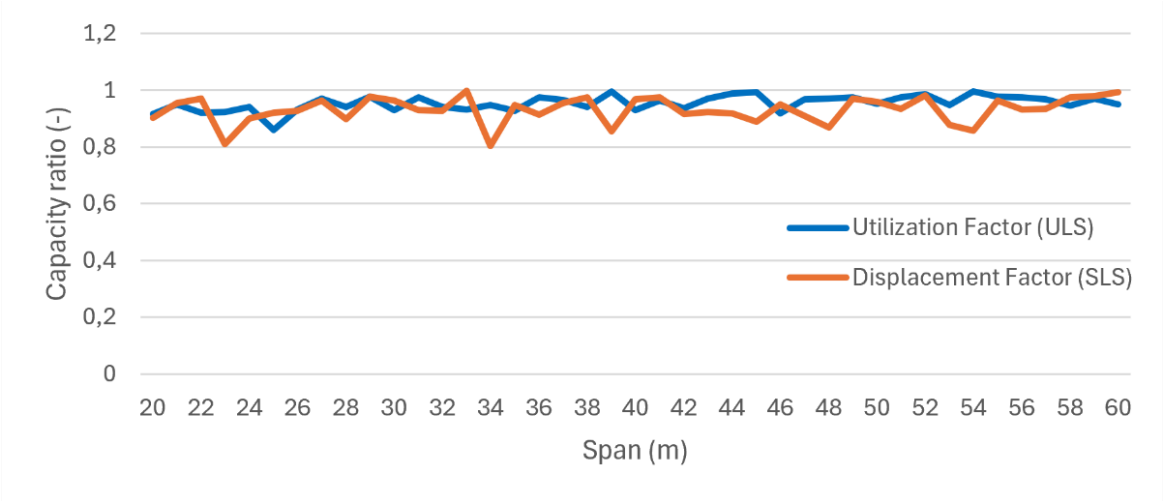

Figure 5.5: Cross-section utilization (ULS) versus vertical displacement (SLS) across the evaluated span range for the Pratt topology (IPE dataset).

6 Discussion

6.1 Solving deflection through global geometry

The sustained efficiency observed in the optimization data (Section 5.4) highlights a significant advantage of the integrated computational workflow over the manual engineering processes. In standard practice, longer bridge spans are typically governed by serviceability limit states (SLS) rather than ultimate strength, with vertical deflection becoming the primary constraint. To satisfy these deflection criteria, human engineers are often forced to select oversized cross-sections with larger moments of inertia to generate sufficient bending stiffness. By doing this the actual stress utilization (ULS) of the steel significantly drops, leading to an inefficient use of material strength. This forced over-dimensioning to satisfy deflection limits is widely referred to as the stiffness penalty.

The evolutionary solver however, successfully bypasses this limitation. The results demonstrate that both the cross-sectional utilization and the displacement factor remain consistently high across the entire 20 to 60-meter span range. Instead of relying on heavier cross-sections to limit deflection, Wallacei adapts the global geometry to generate structural stiffness. As analyzed in Section 5.3, the algorithm adjusts the span-to-height (L/H) ratio to compensate for the increased span.

By resolving the critical deflection constraints through global geometric adjustments, the local cross-section optimizer in Karamba3D is no longer forced to select heavier profiles. Instead, it can consistently assign slender, highly utilized profiles. As a result, this coupled mechanism achieves a fully stressed design, actively preventing the structural over-dimensioning traditionally required to satisfy the stiffness criteria.

6.2 Comparing the L/H ratios to literature

The geometric results of the parametric optimization (Section 5.3) provide a valuable basis for validating existing theoretical rules of thumb within bridge engineering. For the parallel-chord topologies (Pratt and Warren), the span-to-height ratios selected by the algorithm, ranging between 1:13 and 1:16, largely align with conventional literature, which recommends a range of 1:10 to 1:14 for pedestrian bridges. The computational model thereby confirms that these traditional geometric proportions indeed lead to optimal material usage for constant-height designs.

However, a significant deviation occurs with the Parker topology. While the literature recommends a deep midspan ratio of 1:7 to 1:9 for parabolic trusses, the evolutionary solver consistently reduces this height to flatter ratios between 1:10 and 1:13.

The reason for this difference is the type of load. Traditional literature is based on heavy highway bridges, which need a deep arch to handle massive forces. However, for a lightly loaded pedestrian bridge, a deep arch is inefficient. It forces the internal diagonal members to be very long. Long steel members easily buckle under compression, which means they would need to be thicker and heavier to stay stable. By choosing a flatter arch, the algorithm keeps the diagonal members short, preventing buckling and saving a lot of material.

6.3 The mass reduction of hybrid cross-sections

The mass reductions observed in the hybrid datasets (Section 5.2) clearly demonstrate the structural benefit of efficient member utilization. As demonstrated, transitioning from uniform open profiles to a hybrid configuration yielded mass savings of up to 27.5% for the Warren topology. The algorithm prefers Circular Hollow Sections (CHS) for the web members simply because they are much better at resisting buckling.

Open profiles like IPE beams are designed to resist bending, but they easily buckle sideways under compression. Since the web members of a truss primarily experience axial forces, IPE profiles are inefficient there.

CHS tubes, on the other hand, are highly resistant to buckling in any direction because of their round shape. This is exactly why the Warren truss, with its long diagonals, showed the biggest weight savings. It proves that picking the right profile shape for the right force drastically reduces the total amount of material.

6.4 Model limitations

The evolutionary algorithm finds highly efficient shapes, but it still works in a simplified computer environment. To build these bridges in the real world, a few practical limitations of this model must be considered.

6.4.1 Missing wind loads

The current model only calculates vertical forces: the dead weight of the bridge itself and the live load of the pedestrians. In reality bridges must also withstand lateral forces like wind load. Slender trusses, especially the Warren topology with its long diagonals, are very sensitive to sideways bending and vibrations.

If wind loads were included in the calculation, the algorithm would have to adapt the geometry. It would likely need to apply bigger profiles or for example wind bracings to provide enough lateral stiffness. Therefore, the structural masses calculated in Chapter 5 are theoretical minimums. A real, wind-resistant bridge would be heavier.

6.4.2 Idealized joints and connections

In the Grasshopper and Karamba3D model, the connections between the steel members are calculated as perfect, weightless points. In a real construction project, connecting round CHS tubes to flat IPE beams requires heavy steel gusset plates, stiffeners, and a lot of welding.

These physical steel joints add a significant amount of dead weight to the bridge, which is currently ignored in the mass calculations. Additionally, real-world welded joints are not perfectly hinged. This stiffness at the connections creates secondary bending moments in the steel members, which are not accounted for in this computer model.

7 Conclusion & recommendations

7.1 Conclusion

This research investigated the influence of truss topology and geometric proportions on the material efficiency of steel pedestrian bridges. By parametrically optimizing spans ranging from 20 to 60 meters, the computational model successfully generated highly efficient bridge designs that satisfy both strength and stiffness requirements.

To answer the first sub-question regarding the span-to-height ratio, the results confirmed that for constant-height bridges (Pratt and Warren) a ratio between 1:13 and 1:16 is optimal. For parabolic bridges (Parker) a flatter arch proved much more efficient than traditional guidelines suggest. The algorithm showed that adapting these overall geometric proportions is the most efficient way to satisfy strict stiffness limits, preventing the unnecessary material waste of simply using thicker steel profiles.

Regarding the performance of the different topologies (the second sub-question), the optimization revealed that the most efficient shape depends on both the span length and the chosen cross-section. When using slender profiles like IPE, the Parker truss is the most material-efficient across the entire 20 to 60-meter range. However, when using heavier profiles like HEA or HEB, the Warren truss is actually lighter for shorter spans. Despite this variation, a clear universal trend emerged from the data: for any span exceeding 40 meters, the Parker truss consistently becomes the most efficient topology, regardless of the steel profile used.

Finally, regarding the third sub-question, the research demonstrated the massive benefit of using Circular Hollow Sections (CHS) for the web members. Switching from uniform open profiles (I-beams) to a hybrid design, using CHS for the web and I-beams for the chords, reduced the total mass by up to 27.5% for the Warren truss. Because round tubes are highly resistant to axial buckling, the algorithm could use much lighter sections for the web members, while keeping the practical I-beams to support the deck.

Ultimately, while real-world factors like wind loads and heavy steel joints will make a physical bridge heavier, this research proves that optimizing topology, geometric proportions, and profile shapes is a highly effective way to minimize material waste.

7.2 Recommendations

For structural engineers designing pedestrian bridges, it is highly recommended to reconsider standard rules of thumb. Traditional deep-arch guidelines are meant for heavy traffic and lead to inefficient, heavy designs when applied to light pedestrian loads. Additionally, engineers should actively utilize hybrid configurations, combining I-beams for the chords with round CHS tubes for the web members, to prevent buckling and save significant material weight.

For future research and the further development of this computational model, the following steps are recommended:

- **Include lateral wind loads:** The current model should be expanded into a full 3D simulation that calculates lateral wind forces. This would allow the algorithm to optimize wind bracing and deck width, providing a more realistic total mass, especially for slender topologies like the Warren truss.

- **Account for physical steel connections:** By including the mass of gusset plates and calculating the secondary bending moments of real joints, the results will better reflect real-world construction.
- **Add dynamic vibration checks:** Since lightweight pedestrian bridges are highly sensitive to bouncing and resonance, future models should integrate dynamic frequency checks alongside the current vertical strength and stiffness limits.

Appendix A: Full Grasshopper script

A.1 Global overview

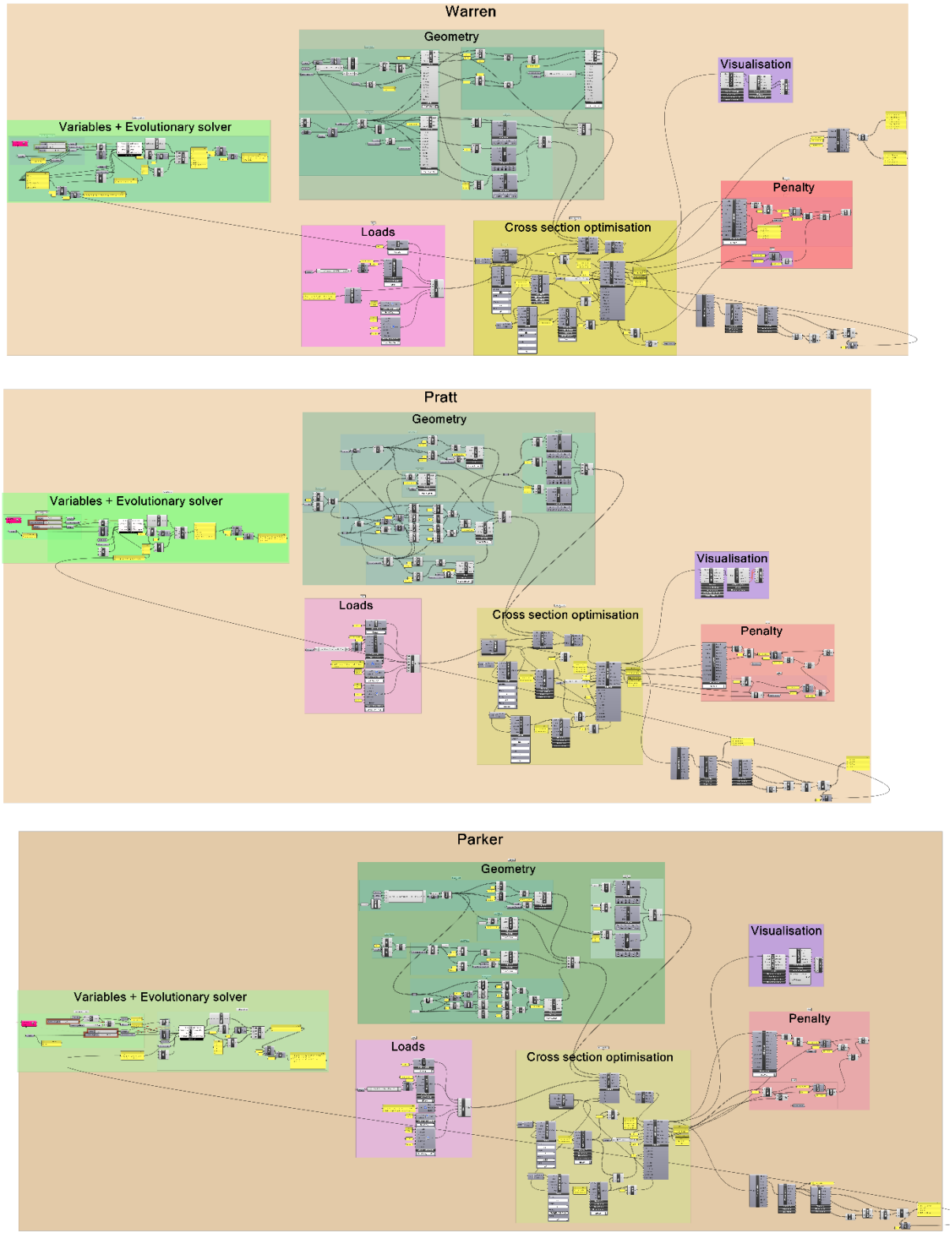

Figure A. 1: Global overview of the parametric Grasshopper definition, illustrating the complete computational setup for the Warren, Pratt, and Parker truss topologies.

A.2 Geometry Pratt

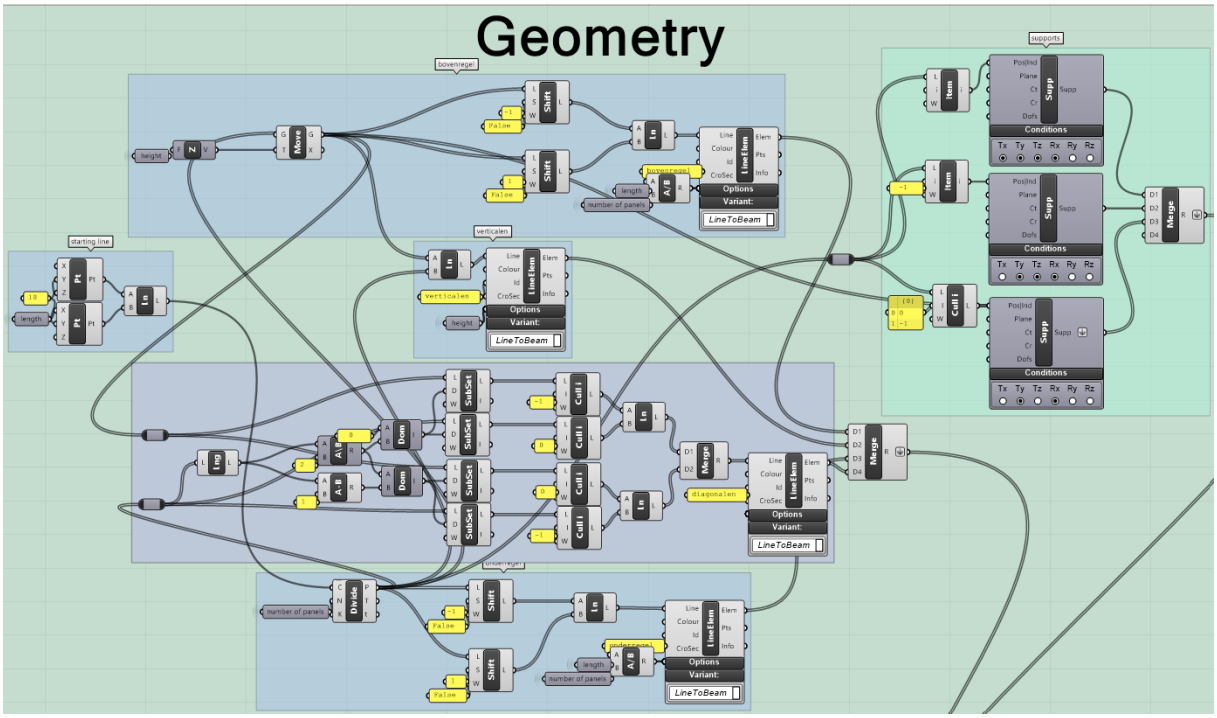

Figure A. 2: Detailed view of the geometric generation logic for the Pratt truss configuration.

A.3 Geometry Warren

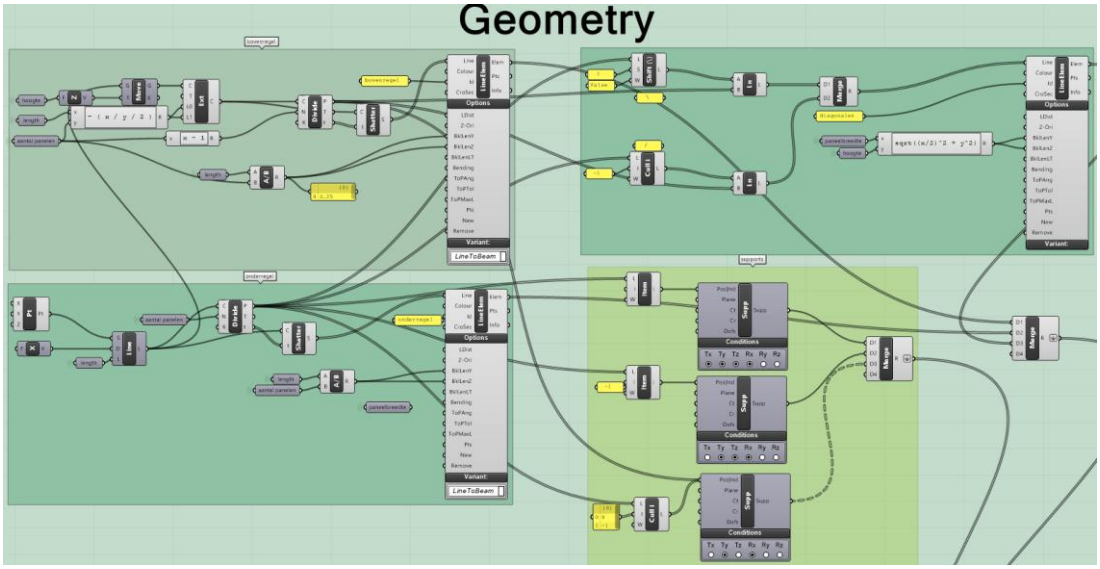

Figure A. 3: Detailed view of the geometric generation logic for the Warren truss configuration.

A.4 Geometry Parker

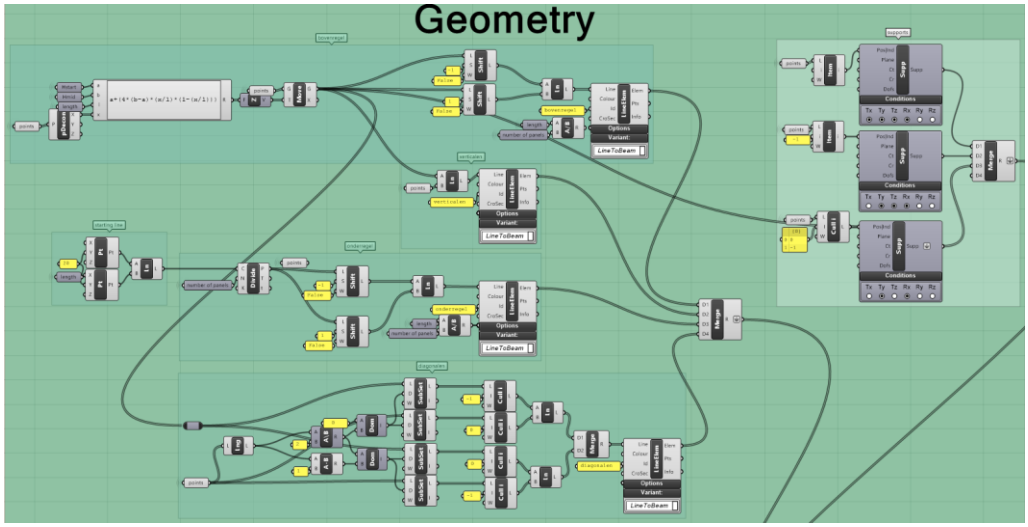

Figure A. 4: Detailed view of the parabolic geometric generation logic for the Parker truss configuration.

A.5 Variables & evolutionary solver

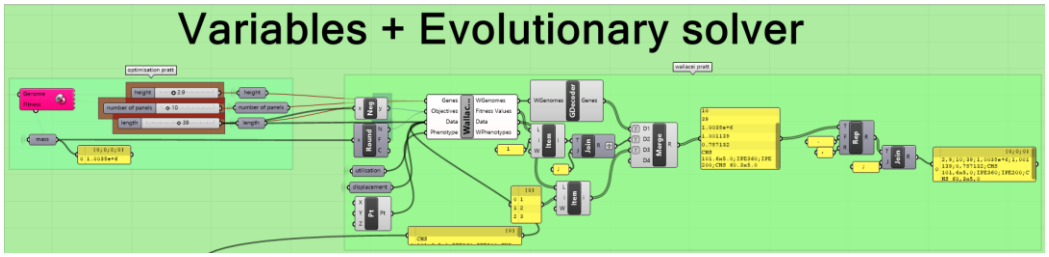

Figure A. 5: Detailed view of the input variables and the Wallacei evolutionary solver setup. (Note: This setup is identical across all three structural topologies).

A.6 Loads

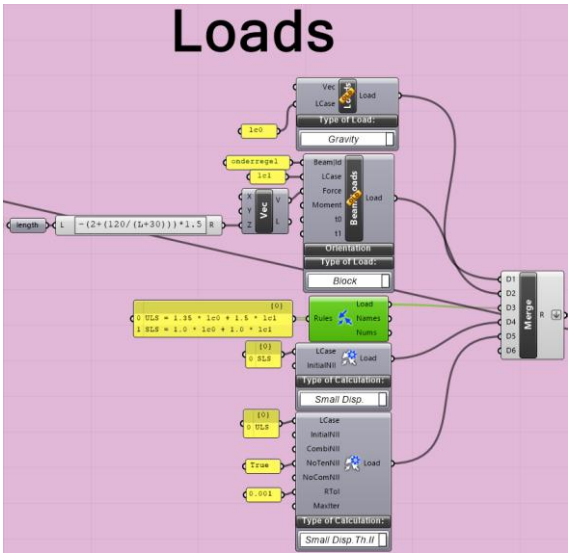

Figure A. 6: Detailed view of the structural load application. (Note: This setup is identical across all three structural topologies).

A.7 Cross section optimalisation

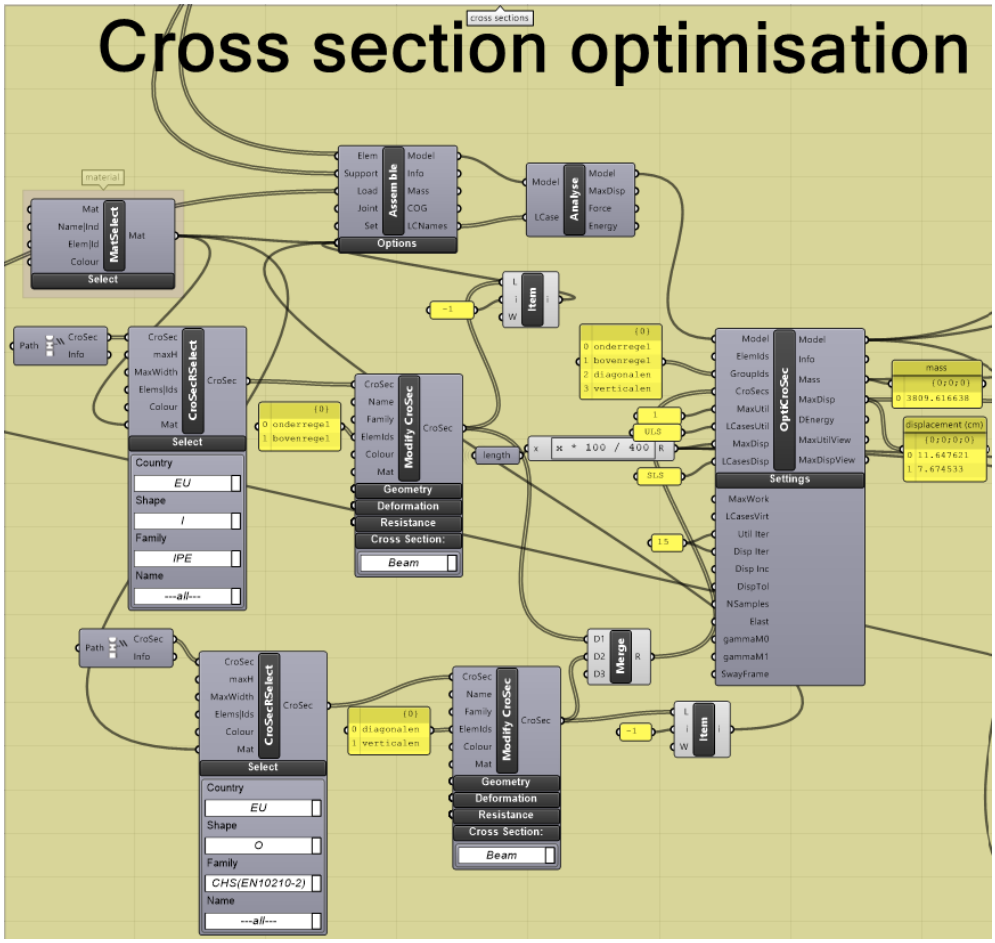

Figure A. 7: Detailed view of the Karamba3D local cross-section optimization logic. (Note: This setup is identical across all three structural topologies).

A.8 Penalty

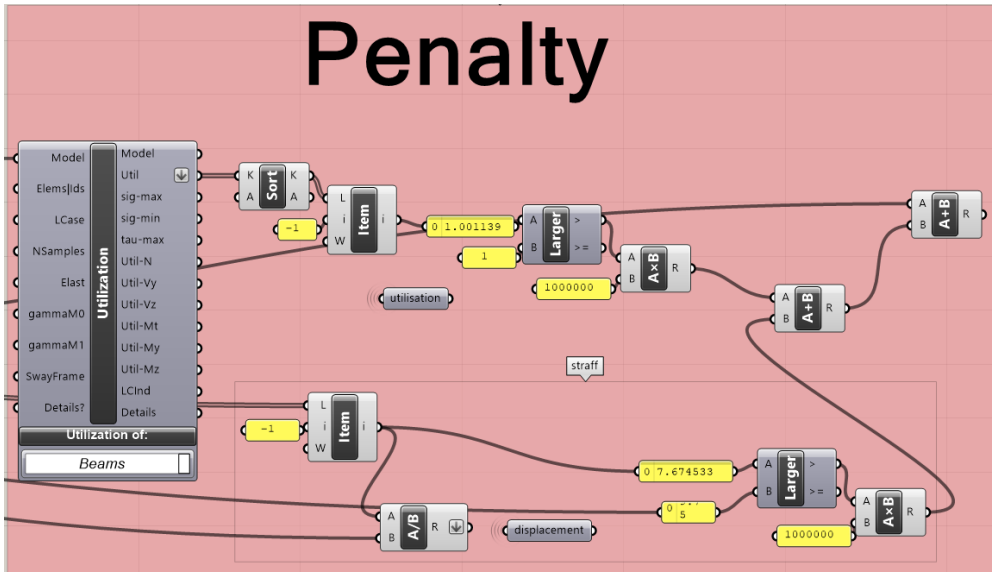

Figure A. 8: Detailed view of the heuristic penalty formulation used to strictly enforce ULS and SLS constraints during the evolutionary process. (Note: This setup is identical across all three structural topologies).

A.9 Visualisation

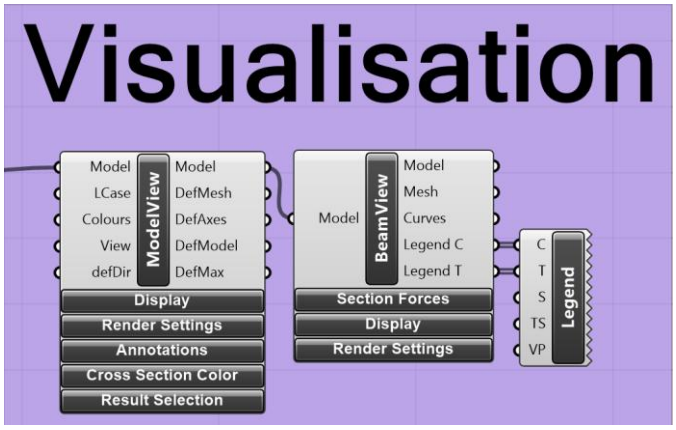

Figure A. 9: Detailed view of the data visualization components. (Note: This setup is identical across all three structural topologies).

Appendix B: Full optimization datasets for all truss topologies

B.1 Pratt

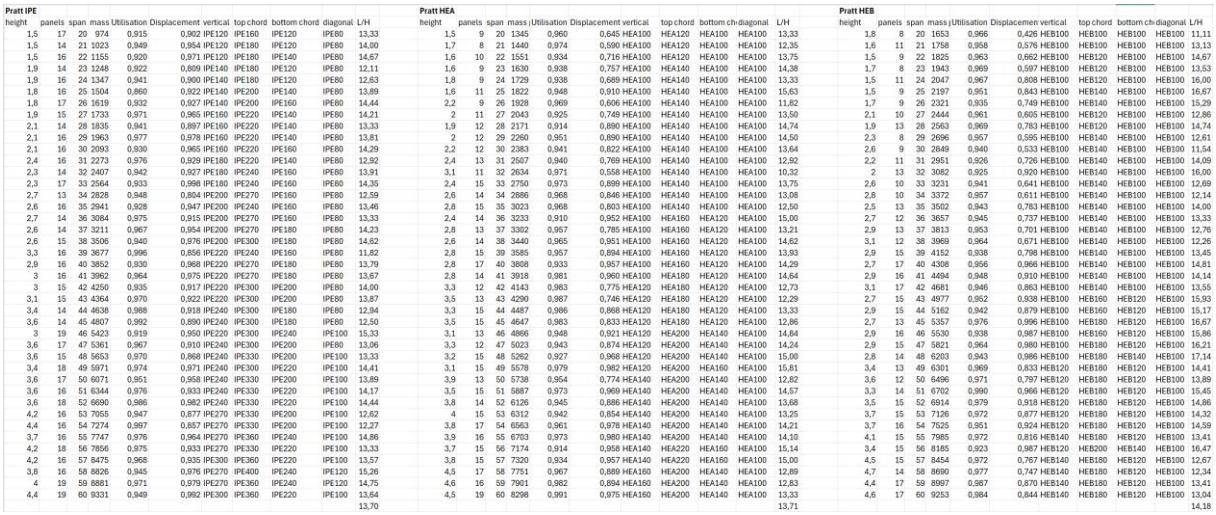

Pratt IPE											
height	panels	span	mass	Utilisation	Displacement	vertical	top chord	bottom chord	diagonal	L/H	
1,5	17	20	974	0,915	0,902	IPE120	IPE160	IPE120	IPE80	13,33	
1,5	14	21	1023	0,949	0,954	IPE120	IPE180	IPE120	IPE80	14,00	
1,5	16	22	1155	0,920	0,971	IPE120	IPE180	IPE140	IPE80	14,67	
1,9	14	23	1248	0,922	0,809	IPE140	IPE180	IPE120	IPE80	12,11	
1,9	16	24	1347	0,941	0,900	IPE140	IPE180	IPE120	IPE80	12,63	
1,8	16	25	1504	0,860	0,922	IPE140	IPE200	IPE140	IPE80	13,89	
1,8	17	26	1619	0,932	0,927	IPE140	IPE200	IPE160	IPE80	14,44	
1,9	15	27	1733	0,971	0,965	IPE160	IPE220	IPE140	IPE80	14,21	
2,1	14	28	1835	0,941	0,897	IPE160	IPE220	IPE140	IPE80	13,33	
2,1	16	29	1963	0,977	0,978	IPE160	IPE220	IPE140	IPE80	13,81	
2,1	16	30	2093	0,930	0,965	IPE160	IPE220	IPE160	IPE80	14,29	
2,4	16	31	2273	0,976	0,929	IPE180	IPE220	IPE140	IPE80	12,92	
2,3	14	32	2407	0,942	0,927	IPE180	IPE240	IPE160	IPE80	13,91	
2,3	17	33	2564	0,933	0,998	IPE180	IPE240	IPE160	IPE80	14,35	
2,7	13	34	2828	0,948	0,804	IPE200	IPE270	IPE160	IPE80	12,59	
2,6	16	35	2941	0,928	0,947	IPE200	IPE240	IPE160	IPE80	13,46	
2,7	14	36	3084	0,975	0,915	IPE200	IPE270	IPE160	IPE80	13,33	
2,6	14	37	3211	0,967	0,954	IPE200	IPE270	IPE180	IPE80	14,23	
2,6	15	38	3506	0,940	0,976	IPE200	IPE300	IPE180	IPE80	14,62	
3,3	16	39	3677	0,996	0,856	IPE220	IPE240	IPE160	IPE80	11,82	
2,9	16	40	3852	0,930	0,968	IPE220	IPE270	IPE180	IPE80	13,79	
3	16	41	3962	0,964	0,975	IPE220	IPE270	IPE180	IPE80	13,67	
3	15	42	4250	0,935	0,917	IPE220	IPE300	IPE200	IPE80	14,00	
3,1	15	43	4364	0,970	0,922	IPE220	IPE300	IPE200	IPE80	13,87	
3,4	14	44	4638	0,988	0,918	IPE240	IPE300	IPE180	IPE80	12,94	
3,6	14	45	4807	0,992	0,890	IPE240	IPE300	IPE180	IPE80	12,50	
3	19	46	5423	0,919	0,950	IPE220	IPE300	IPE240	IPE100	15,33	
3,6	17	47	5361	0,967	0,910	IPE240	IPE300	IPE200	IPE80	13,06	
3,6	15	48	5653	0,970	0,868	IPE240	IPE330	IPE200	IPE100	13,33	
3,4	18	49	5971	0,974	0,971	IPE240	IPE300	IPE220	IPE100	14,41	
3,6	17	50	6071	0,951	0,958	IPE240	IPE330	IPE200	IPE100	13,89	
3,6	16	51	6344	0,976	0,933	IPE240	IPE330	IPE220	IPE100	14,17	
3,6	18	52	6690	0,986	0,982	IPE240	IPE330	IPE220	IPE100	14,44	
4,2	16	53	7055	0,947	0,877	IPE270	IPE330	IPE200	IPE100	12,62	
4,4	16	54	7274	0,997	0,857	IPE270	IPE330	IPE200	IPE100	12,27	
3,7	16	55	7747	0,976	0,964	IPE270	IPE360	IPE240	IPE100	14,86	
4,2	18	56	7856	0,975	0,933	IPE270	IPE330	IPE220	IPE100	13,33	
4,2	16	57	8475	0,968	0,935	IPE300	IPE360	IPE220	IPE100	13,57	
3,8	16	58	8826	0,945	0,976	IPE270	IPE400	IPE240	IPE120	15,26	
4	19	59	8881	0,971	0,979	IPE270	IPE360	IPE240	IPE120	14,75	
4,4	19	60	9331	0,949	0,992	IPE300	IPE360	IPE220	IPE100	13,64	
										13,70	

Pratt HEA											
height	panels	span	mass	Utilisation	Displacement	vertical	top chord	bottom chord	diagonal	L/H	
1,5	9	20	1345	0,960	0,645	HEA100	HEA120	HEA100	HEA100	13,33	
1,7	8	21	1440	0,974	0,590	HEA100	HEA120	HEA100	HEA100	12,35	
1,6	10	22	1551	0,934	0,716	HEA100	HEA120	HEA100	HEA100	13,75	
1,6	9	23	1630	0,938	0,757	HEA100	HEA140	HEA100	HEA100	14,38	
1,8	9	24	1729	0,938	0,689	HEA100	HEA140	HEA100	HEA100	13,33	
1,6	11	25	1822	0,948	0,910	HEA100	HEA140	HEA100	HEA100	15,63	
2,2	9	26	1928	0,969	0,606	HEA100	HEA140	HEA100	HEA100	11,82	
2	11	27	2043	0,925	0,749	HEA100	HEA140	HEA100	HEA100	13,50	
1,9	12	28	2171	0,914	0,890	HEA100	HEA140	HEA100	HEA100	14,74	
2	12	29	2260	0,951	0,890	HEA100	HEA140	HEA100	HEA100	14,50	
2,2	12	30	2383	0,941	0,822	HEA100	HEA140	HEA100	HEA100	13,64	
2,4	13	31	2507	0,940	0,769	HEA100	HEA140	HEA100	HEA100	12,92	
3,1	11	32	2634	0,971	0,558	HEA100	HEA140	HEA100	HEA100	10,32	
2,4	15	33	2750	0,973	0,899	HEA100	HEA140	HEA100	HEA100	13,75	
2,6	14	34	2886	0,968	0,846	HEA100	HEA140	HEA100	HEA100	13,08	
2,8	15	35	3023	0,968	0,803	HEA100	HEA140	HEA100	HEA100	12,50	
2,4	14	36	3233	0,910	0,952	HEA100	HEA160	HEA120	HEA100	15,00	
2,8	13	37	3302	0,957	0,785	HEA100	HEA160	HEA120	HEA100	13,21	
2,6	14	38	3440	0,965	0,951	HEA100	HEA160	HEA120	HEA100	14,62	
2,8	15	39	3585	0,957	0,894	HEA100	HEA160	HEA120	HEA100	13,93	
2,8	17	40	3808	0,933	0,957	HEA100	HEA160	HEA120	HEA100	14,29	
2,8	14	41	3918	0,981	0,960	HEA100	HEA180	HEA120	HEA100	14,64	
3,3	12	42	4143	0,983	0,775	HEA120	HEA180	HEA120	HEA100	12,73	
3,5	13	43	4290	0,987	0,746	HEA120	HEA180	HEA120	HEA100	12,29	
3,3	15	44	4487	0,986	0,868	HEA120	HEA180	HEA120	HEA100	13,33	
3,5	15	45	4647	0,983	0,833	HEA120	HEA180	HEA120	HEA100	12,86	
3,1	13	46	4866	0,948	0,921	HEA120	HEA200	HEA140	HEA100	14,84	
3,3	12	47	5023	0,943	0,874	HEA120	HEA200	HEA140	HEA100	14,24	
3,2	15	48	5262	0,927	0,968	HEA120	HEA200	HEA140	HEA100	15,00	
3,1	15	49	5578	0,979	0,982	HEA120	HEA200	HEA160	HEA100	15,81	
3,9	13	50	5738	0,954	0,774	HEA140	HEA200	HEA140	HEA100	12,82	
3,5	15	51	5887	0,973	0,969	HEA140	HEA200	HEA140	HEA100	14,57	
3,8	14	52	6126	0,945	0,886	HEA140	HEA200	HEA140	HEA100	13,68	
4	15	53	6312	0,942	0,854	HEA140	HEA200	HEA140	HEA100	13,25	
3,8	17	54	6563	0,961	0,978	HEA140	HEA200	HEA140	HEA100	14,21	
3,9	16	55	6703	0,973	0,980	HEA140	HEA200	HEA140	HEA100	14,10	
3,7	15	56	7174	0,914	0,958	HEA140	HEA220	HEA160	HEA100	15,14	
3,8	15	57	7320	0,934	0,957	HEA140	HEA220	HEA160	HEA100	15,00	
4,5	17	58	7751	0,967	0,889	HEA160	HEA200	HEA140	HEA100	12,89	
4,6	16	59	7901	0,982	0,894	HEA160	HEA200	HEA140	HEA100	12,83	
4,5	19	60	8298	0,991	0,975	HEA160	HEA200	HEA140	HEA100	13,33	
										13,71	

Pratt HEB											
height	panels	span	mass	Utilisation	Displacement	vertical	top chord	bottom chord	diagonal	L/H	
1,8	8	20	1653	0,966	0,426	HEB100	HEB100	HEB100	HEB100	11,11	
1,6	11	21	1758	0,958	0,576	HEB100	HEB100	HEB100	HEB100	13,13	
1,5	9	22	1825	0,963	0,662	HEB100	HEB120	HEB100	HEB100	14,67	
1,7	8	23	1943	0,969	0,597	HEB100	HEB120	HEB100	HEB100	13,53	
1,5	11	24	2047	0,967	0,808	HEB100	HEB120	HEB100	HEB100	16,00	
1,5	9	25	2197	0,951	0,843	HEB100	HEB140	HEB100	HEB100	16,67	
1,7	9	26	2321	0,935	0,749	HEB100	HEB140	HEB100	HEB100	15,29	
2,1	10	27	2444	0,961	0,605	HEB100	HEB120	HEB100	HEB100	12,86	
1,9	13	28	2563	0,969	0,783	HEB100	HEB120	HEB100	HEB100	14,74	
2,3	8	29	2696	0,957	0,595	HEB100	HEB140	HEB100	HEB100	12,61	
2,6	9	30	2849	0,940	0,533	HEB100	HEB140	HEB100	HEB100	11,54	
2,2	11	31	2951	0,926	0,726	HEB100	HEB140	HEB100	HEB100	14,09	
2	13	32	3082	0,925	0,920	HEB100	HEB140	HEB100	HEB100	16,00	
2,6	10	33	3231	0,941	0,641	HEB100	HEB140	HEB100	HEB100	12,69	
2,8	10	34	3372	0,957	0,611	HEB100	HEB140	HEB100	HEB100	12,14	
2,5	13	35	3502	0,943	0,783	HEB100	HEB140	HEB100	HEB100	14,00	
2,7	12	36	3657	0,945	0,737	HEB100	HEB140	HEB100	HEB100	13,33	
2,9	13	37	3813	0,953	0,701	HEB100	HEB140	HEB100	HEB100	12,76	
3,1	12	38	3969	0,964	0,671	HEB100	HEB140	HEB100	HEB100	12,26	
2,9	15	39	4152	0,938	0,798	HEB100	HEB140	HEB100	HEB100	13,45	
2,7	17	40	4308	0,956	0,966	HEB100	HEB140	HEB100	HEB100	14,81	
2,9	16	41	4494	0,948	0,910	HEB100	HEB140	HEB100	HEB100	14,14	
3,1	17	42	4681	0,946	0,863	HEB100	HEB140	HEB100	HEB100	13,55	
2,7	15	43	4977	0,952	0,938	HEB100	HEB160	HEB120	HEB100	15,93	
2,9	15	44	5162	0,942	0,879	HEB100	HEB160	HEB120	HEB100	15,17	
2,7	13	45	5357	0,976	0,996	HEB100	HEB180	HEB120	HEB100	16,67	
2,9	16	46	5530	0,938	0,987	HEB100	HEB160	HEB120	HEB100	15,86	
2,9	15	47	5821	0,964	0,980	HEB100	HEB180	HEB120	HEB100	16,21	
2,8	14	48	6203	0,943	0,986	HEB100	HEB180	HEB140	HEB100	17,14	
3,4	13	49	6301	0,969	0,833	HEB100	HEB180	HEB120	HEB100	14,41	
3,6	12	50	6496	0,971	0,797	HEB100	HEB180	HEB120	HEB100	13,89	
3,3	14	51	6702	0,990	0,966	HEB100	HEB180	HEB120	HEB100	15,45	
3,5	15	52	6914	0,979	0,918	HEB100	HEB180	HEB120	HEB100	14,86	
3,7	15	53	7126	0,972	0,877	HEB100	HEB180	HEB120	HEB100	14,32	
3,7	16	54	7525	0,951	0,924	HEB100	HEB180	HEB120	HEB100	14,59	
4,1	15	55	7985	0,972	0,816	HEB100	HEB180	HEB120	HEB100	13,41	
3,4	15	56	8185	0,923	0,987	HEB100	HEB200	HEB140	HEB100	16,47	
4,5	15	57	8454	0,972	0,767	HEB100	HEB180	HEB120	HEB100	12,67	
4,7	14	58	8690	0,977	0,747	HEB100	HEB180	HEB120	HEB100	12,34	
4,4	17	59	8997	0,987	0,870	HEB100	HEB180	HEB120	HEB100	13,41	
4,6	17	60	9253	0,984	0,844	HEB100	HEB180	HEB120	HEB100	13,04	
										14,18	

Figure B. 1: Optimized geometric variables and cross-sectional profiles for the Pratt uniform IPE, HEA and HEB configuration.

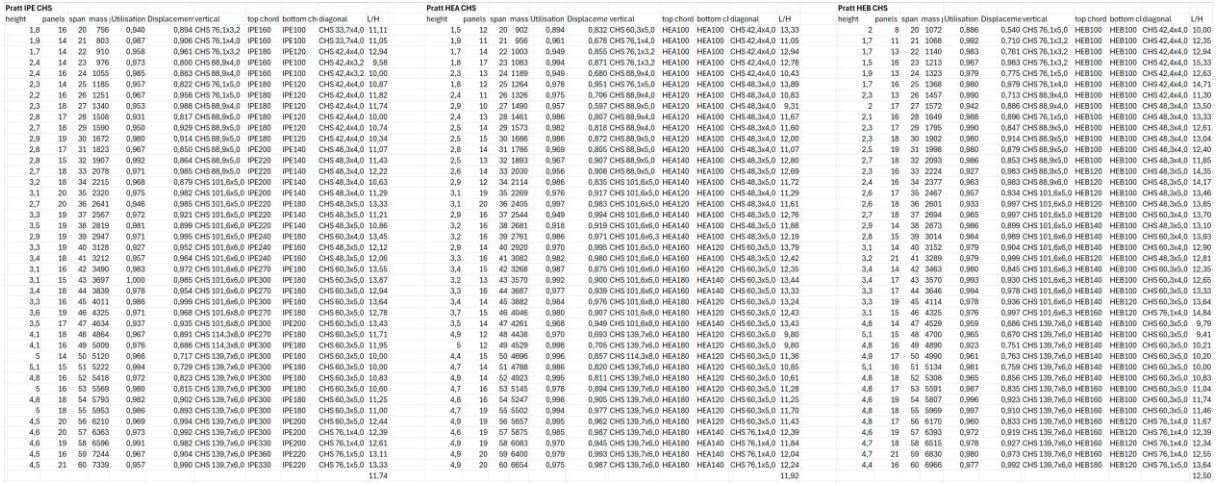

Pratt IPE CHS											
height	panels	span	mass	Utilisation	Displacement	vertical	top chord	bottom chord	diagonal	L/H	
1,8	16	20	756	0,940	0,894	CHS 76,1x3,2	IPE160	IPE100	CHS 33,7x4,0	11,11	
1,9	14	21	803	0,987	0,906	CHS 76,1x4,0	IPE160	IPE100	CHS 33,7x4,0	11,05	
1,7	14	22	910	0,958	0,961	CHS 76,1x3,2	IPE180	IPE120	CHS 42,4x4,0	12,94	
2,4	14	23	976	0,973	0,800	CHS 88,9x4,0	IPE160	IPE100	CHS 42,4x3,2	9,58	
2,4	16	24	1055	0,985	0,883	CHS 88,9x4,0	IPE160	IPE100	CHS 42,4x3,2	10,00	
2,3	14	25	1185	0,957	0,822	CHS 76,1x5,0	IPE180	IPE120	CHS 42,4x4,0	10,87	
2,2	16	26	1251	0,967	0,956	CHS 76,1x5,0	IPE180	IPE120	CHS 42,4x4,0	11,82	
2,3	18	27	1340	0,953	0,988	CHS 88,9x4,0	IPE180	IPE120	CHS 42,4x4,0	11,74	
2,8	17	28	1508	0,931	0,817	CHS 88,9x5,0	IPE180	IPE120	CHS 42,4x4,0	10,00	
2,7	18	29	1590	0,950	0,929	CHS 88,9x5,0	IPE180	IPE120	CHS 42,4x4,0	10,74	
2,9	19	30	1672	0,980	0,914	CHS 88,9x5,0	IPE180	IPE120	CHS 42,4x4,0	10,34	
2,8	17	31	1823	0,967	0,850	CHS 88,9x5,0	IPE200	IPE140	CHS 48,3x4,0	11,07	
2,8	15	32	1907	0,992	0,864	CHS 88,9x5,0	IPE220	IPE140	CHS 48,3x4,0	11,43	
2,7	18	33	2078	0,971	0,985	CHS 88,9x5,0	IPE220	IPE140	CHS 48,3x4,0	12,22	
3,2	18	34	2215	0,968	0,879	CHS 101,6x5,0	IPE200	IPE140	CHS 48,3x4,0	10,63	
3,1	20	35	2320	0,975	0,982	CHS 101,6x5,0	IPE200	IPE140	CHS 48,3x4,0	11,29	
2,7	20	36	2641	0,946	0,985	CHS 101,6x5,0	IPE220	IPE180	CHS 48,3x5,0	13,33	
3,3	19	37	2567	0,972	0,921	CHS 101,6x5,0	IPE220	IPE140	CHS 48,3x5,0	11,21	
3,5	19	38	2819	0,981	0,899	CHS 101,6x6,0	IPE220	IPE140	CHS 48,3x5,0	10,86	
2,9	19	39	2947	0,971	0,995	CHS 101,6x5,0	IPE240	IPE180	CHS 60,3x4,0	13,45	
3,3	19	40	3128	0,927	0,952	CHS 101,6x6,0	IPE240	IPE180	CHS 48,3x5,0	12,12	
3,4	18	41	3212	0,957	0,964	CHS 101,6x6,0	IPE240	IPE160	CHS 48,3x5,0	12,06	
3,1	16	42	3490	0,983	0,972	CHS 101,6x6,0	IPE270	IPE180	CHS 60,3x5,0	13,55	
3,1	15	43	3697	1,000	0,985	CHS 101,6x6,0	IPE300	IPE180	CHS 60,3x5,0	13,67	
3,4	18	44	3839	0,978	0,954	CHS 101,6x6,0	IPE270	IPE180	CHS 60,3x5,0	12,94	
3,3	16	45	4011	0,986	0,999	CHS 101,6x6,0	IPE300	IPE180	CHS 60,3x5,0	13,64	
3,6	19	46	4325	0,971	0,968	CHS 101,6x8,0	IPE270	IPE180	CHS 60,3x5,0	12,78	
3,5	17	47	4634	0,937	0,935	CHS 101,6x8,0	IPE300	IPE200	CHS 60,3x5,0	13,43	
4,1	18	48	4864	0,967	0,891	CHS 114,3x8,0	IPE270	IPE180	CHS 60,3x5,0	11,71	
4,1	16	49	5009	0,976	0,886	CHS 114,3x8,0	IPE300	IPE180	CHS 60,3x5,0	11,95	
5	14	50	5120	0,966	0,717	CHS 139,7x6,0	IPE300	IPE180	CHS 60,3x5,0	10,00	
5,1	15	51	5222	0,994	0,729	CHS 139,7x6,0	IPE300	IPE180	CHS 60,3x5,0	10,00	
4,8	16	52	5418	0,972	0,823	CHS 139,7x6,0	IPE300	IPE180	CHS 60,3x5,0	10,83	
5	16	53	5569	0,989	0,815	CHS 139,7x6,0	IPE300	IPE180	CHS 60,3x5,0	10,60	
4,8	18	54	5793	0,982	0,902	CHS 139,7x6,0	IPE300	IPE180	CHS 60,3x5,0	11,25	
5	18	55	5953	0,986	0,893	CHS 139,7x6,0	IPE300	IPE180	CHS 60,3x5,0	11,00	
4,5	20	56	6210	0,969	0,994	CHS 139,7x6,0	IPE300	IPE200	CHS 60,3x5,0	12,44	
4,6	20	57	6363	0,973	0,992	CHS 139,7x6,0	IPE300	IPE200	CHS 76,1x4,0	12,39	
4,6	19	58	6596	0,991	0,982	CHS 139,7x6,0	IPE330	IPE200	CHS 76,1x4,0	12,61	
4,5	16	59	7244	0,967	0,904	CHS 139,7x6,0	IPE360	IPE220	CHS 76,1x5,0	13,11	
4,5	21	60	7339	0,957	0,990	CHS 139,7x6,0	IPE330	IPE220	CHS 76,1x5,0	13,33	
										11,74	

Pratt HEA CHS											
height	panels	span	mass	Utilisation	Displacement	vertical	top chord	bottom chord	diagonal	L/H	
1,5	12	20	902	0,894	0,832	CHS 60,3x5,0	HEA100	HEA100	CHS 42,4x4,0	13,33	
1,9	11	21	956	0,961	0,678	CHS 76,1x4,0	HEA100	HEA100	CHS 42,4x4,0	11,05	
1,7	14	22	1003	0,949	0,855	CHS 76,1x3,2	HEA100	HEA100	CHS 42,4x4,0	12,94	
1,8	17	23	1083	0,994	0,871	CHS 76,1x3,2	HEA100	HEA100	CHS 42,4x4,0	12,78	
2,3	13	24	1189	0,949	0,680	CHS 88,9x4,0	HEA100	HEA100	CHS 42,4x4,0	10,43	
1,8	12	25	1264	0,976	0,951	CHS 76,1x5,0	HEA120	HEA100	CHS 48,3x4,0	13,89	
2,4	11	26	1326	0,975	0,706	CHS 88,9x4,0	HEA120	HEA100	CHS 48,3x4,0	10,83	
2,9	10	27	1490	0,957	0,597	CHS 88,9x5,0	HEA120	HEA100	CHS 48,3x4,0	9,31	
2,4	13	28	1461	0,986	0,807	CHS 88,9x4,0	HEA120	HEA100	CHS 48,3x4,0	11,67	
2,5	14	29	1573	0,982	0,818	CHS 88,9x4,0	HEA120	HEA100	CHS 48,3x4,0	11,60	
2,5	15	30	1686	0,986	0,872	CHS 88,9x5,0	HEA120	HEA100	CHS 48,3x4,0	12,00	
2,8	14	31	1786	0,969	0,805	CHS 88,9x5,0	HEA120	HEA100	CHS 48,3x4,0	11,07	
2,5	13	32	1893	0,967	0,907	CHS 88,9x5,0	HEA140	HEA100	CHS 48,3x5,0	12,80	
2,6	14	33	2030	0,956	0,908	CHS 88,9x5,0	HEA140	HEA100	CHS 48,3x5,0	12,69	
2,9	12	34	2114	0,986	0,835	CHS 101,6x5,0	HEA140	HEA100	CHS 48,3x5,0	11,72	
3,1	19	35	2269	0,976	0,917	CHS 101,6x5,0	HEA120	HEA100	CHS 48,3x4,0	11,29	
3,1	20	36	2405	0,997	0,983	CHS 101,6x5,0	HEA120	HEA100	CHS 48,3x4,0	11,61	
2,9	16	37	2544	0,949	0,994	CHS 101,6x6,0	HEA140	HEA100	CHS 48,3x5,0	12,76	
3,2	16	38	2681	0,916	0,919	CHS 101,6x6,0	HEA140	HEA100	CHS 48,3x5,0	11,88	
3,2	16	39	2761	0,986	0,971	CHS 101,6x6,3	HEA140	HEA100	CHS 48,3x5,0	12,19	
2,9	14	40	2920	0,970	0,995	CHS 101,6x5,0	HEA160	HEA120	CHS 60,3x5,0	13,79	
3,3	16	41	3082	0,982	0,980	CHS 101,6x6,0	HEA160	HEA100	CHS 48,3x5,0	12,42	
3,4	15	42	3268	0,987	0,875	CHS 101,6x6,0	HEA160	HEA120	CHS 60,3x5,0	12,35	
3,2	13	43	3570	0,992	0,900	CHS 101,6x6,0	HEA160	HEA140	CHS 60,3x5,0	13,44	
3,3	16	44	3687	0,977	0,939	CHS 101,6x6,0	HEA160	HEA140	CHS 60,3x5,0	13,33	
3,4	14	45	3882	0,984	0,976	CHS 101,6x8,0	HEA180	HEA120	CHS 60,3x5,0	13,24	
3,7	15	46	4046	0,980	0,907	CHS 101,6x8,0	HEA180	HEA120	CHS 60,3x5,0	12,43	
3,5	14	47	4261	0,968	0,949	CHS 101,6x8,0	HEA180	HEA140	CHS 60,3x5,0	13,43	
4,9	12	48	4438	0,970	0,893	CHS 139,7x6,0	HEA180	HEA120	CHS 60,3x5,0	9,80	
5	12	49	4529	0,998	0,765	CHS 139,7x6,0	HEA180	HEA120	CHS 60,3x5,0	9,80	
4,4	15	50	4696	0,996	0,857	CHS 114,3x8,0	HEA180	HEA120	CHS 60,3x5,0	11,36	
4,7	14	51	4788	0,986	0,820	CHS 139,7x6,0	HEA180	HEA120	CHS 60,3x5,0	10,85	
4,9	14	52	4923	0,995	0,811	CHS 139,7x6,0	HEA180	HEA120	CHS 60,3x5,0	10,61	
4,7	16	53	5145	0,978	0,894	CHS 139,7x6,0	HEA180	HEA120	CHS 60,3x5,0	11,28	
4,8	16	54	5247	0,998	0,905	CHS 139,7x6,0	HEA180	HEA120	CHS 60,3x5,0	11,25	
4,7	19	55	5502	0,994	0,977	CHS 139,7x6,0	HEA180	HEA120	CHS 60,3x5,0	11,70	
4,9	19	56	5657	0,995	0,962	CHS 139,7x6,0	HEA180	HEA120	CHS 60,3x5,0	11,43	
4,6	19	57	5875	0,985	0,987	CHS 139,7x6,0	HEA180	HEA140	CHS 76,1x4,0	12,39	
4,9	19	58	6083	0,970	0,945	CHS 139,7x6,0	HEA180	HEA140	CHS 76,1x4,0	11,84	
4,9	20	59	6400	0,979	0,993	CHS 139,7x6,0	HEA180	HEA140	CHS 76,1x4,0	12,04	
4,9	20	60	6654	0,975	0,987	CHS 139,7x6,0	HEA180	HEA140	CHS 76,1x5,0	12,24	
										11,92	

Pratt HEB CHS											
height	panels	span	mass	Utilisation	Displacement	vertical	top chord	bottom chord	diagonal	L/H	
2	8	20	1072	0,886	0,540	CHS 76,1x5,0	HEB100	HEB100	CHS 42,4x4,0	10,00	
1,7	11	21	1068	0,992	0,710	CHS 76,1x3,2	HEB100	HEB100	CHS 42,4x4,0	12,35	
1,7	13	22	1140	0,983	0,761	CHS 76,1x3,2	HEB100	HEB100	CHS 42,4x4,0	12,94	
1,5	16	23	1213	0,967	0,983	CHS 76,1x3,2	HEB100	HEB100	CHS 42,4x4,0	15,33	
1,9	13	24	1323	0,979	0,775	CHS 76,1x5,0	HEB100	HEB100	CHS 42,4x4,0	12,63	
1,7	16	25	1368	0,980	0,979	CHS 76,1x4,0	HEB100	HEB100	CHS 42,4x4,0	14,71	
2,3	13	26	1457	0,990	0,713	CHS 88,9x4,0	HEB100	HEB100	CHS 42,4x4,0	11,30	
2	17	27	1572	0,942	0,886	CHS 88,9x4,0	HEB100	HEB100	CHS 48,3x4,0	13,50	
2,1	16	28	1649	0,988	0,896	CHS 76,1x5,0	HEB100	HEB100	CHS 48,3x4,0	13,33	
2,3	17	29	1795	0,990	0,847	CHS 88,9x5,0	HEB100	HEB100	CHS 48,3x4,0	12,61	
2,3	18	30	1902	0,980	0,914	CHS 88,9x5,0	HEB100	HEB100	CHS 48,3x4,0	13,04	
2,5	19	31	1996	0,980	0,879	CHS 88,9x5,0	HEB100	HEB100	CHS 48,3x4,0	12,40	
2,7

B.2 Warren

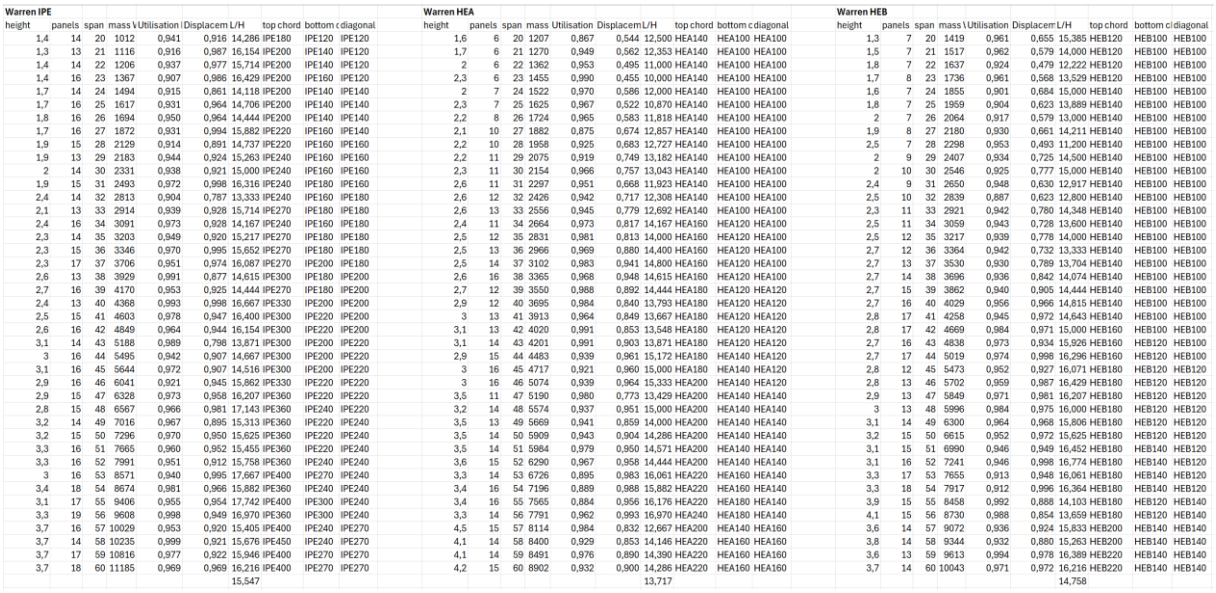

Warren IPE											Warren HEA										Warren HEB									
height	panels	span	mass	Utilisation	Displacem	L/H	top chord	bottom c	diagonal		height	panels	span	mass	Utilisation	Displacem	L/H	top chord	bottom c	diagonal	height	panels	span	mass	Utilisation	Displacem	L/H	top chord	bottom c	diagonal	
1,4	14	20	1012	0,941	0,916	14,286	IPE180	IPE120	IPE120		1,6	6	20	1207	0,867	0,544	12,500	HEA140	HEA100	HEA100	1,3	7	20	1419	0,961	0,655	15,385	HEB120	HEB100	HEB100
1,3	13	21	1116	0,916	0,987	16,154	IPE200	IPE140	IPE120		1,7	6	21	1270	0,949	0,562	12,353	HEA140	HEA100	HEA100	1,5	7	21	1517	0,962	0,579	14,000	HEB120	HEB100	HEB100
1,4	14	22	1206	0,937	0,977	15,714	IPE200	IPE140	IPE120		2	6	22	1362	0,953	0,495	11,000	HEA140	HEA100	HEA100	1,8	7	22	1637	0,924	0,479	12,222	HEB120	HEB100	HEB100
1,4	16	23	1367	0,907	0,986	16,429	IPE200	IPE160	IPE120		2,3	6	23	1455	0,990	0,455	10,000	HEA140	HEA100	HEA100	1,7	8	23	1736	0,961	0,568	13,529	HEB120	HEB100	HEB100
1,7	14	24	1494	0,915	0,861	14,118	IPE200	IPE140	IPE140		2	7	24	1522	0,970	0,586	12,000	HEA140	HEA100	HEA100	1,6	7	24	1855	0,901	0,684	15,000	HEB140	HEB100	HEB100
1,7	16	25	1617	0,931	0,964	14,706	IPE200	IPE140	IPE140		2,3	7	25	1625	0,967	0,522	10,870	HEA140	HEA100	HEA100	1,8	7	25	1959	0,904	0,623	13,889	HEB140	HEB100	HEB100
1,8	16	26	1694	0,950	0,964	14,444	IPE200	IPE140	IPE140		2,2	8	26	1724	0,965	0,583	11,818	HEA140	HEA100	HEA100	2	7	26	2064	0,917	0,579	13,000	HEB140	HEB100	HEB100
1,7	16	27	1872	0,931	0,994	15,882	IPE220	IPE160	IPE140		2,1	10	27	1882	0,875	0,674	12,857	HEA140	HEA100	HEA100	1,9	8	27	2180	0,930	0,661	14,211	HEB140	HEB100	HEB100
1,9	15	28	2129	0,914	0,891	14,737	IPE220	IPE160	IPE160		2,2	10	28	1958	0,925	0,683	12,727	HEA140	HEA100	HEA100	2,5	7	28	2298	0,953	0,493	11,200	HEB140	HEB100	HEB100
1,9	13	29	2183	0,944	0,924	15,263	IPE240	IPE160	IPE160		2,2	11	29	2075	0,919	0,749	13,182	HEA140	HEA100	HEA100	2	9	29	2407	0,934	0,725	14,500	HEB140	HEB100	HEB100
2	14	30	2331	0,938	0,921	15,000	IPE240	IPE160	IPE160		2,3	11	30	2154	0,966	0,757	13,043	HEA140	HEA100	HEA100	2	10	30	2546	0,925	0,777	15,000	HEB140	HEB100	HEB100
1,9	15	31	2493	0,972	0,998	16,316	IPE240	IPE180	IPE160		2,6	11	31	2297	0,951	0,668	11,923	HEA140	HEA100	HEA100	2,4	9	31	2650	0,948	0,630	12,917	HEB140	HEB100	HEB100
2,4	14	32	2813	0,904	0,787	13,333	IPE240	IPE160	IPE180		2,6	12	32	2426	0,942	0,717	12,308	HEA140	HEA100	HEA100	2,5	10	32	2839	0,887	0,623	12,800	HEB140	HEB100	HEB100
2,1	13	33	2914	0,939	0,928	15,714	IPE270	IPE180	IPE180		2,6	13	33	2556	0,945	0,779	12,692	HEA140	HEA100	HEA100	2,3	11	33	2921	0,942	0,780	14,348	HEB140	HEB100	HEB100
2,4	16	34	3091	0,973	0,928	14,167	IPE240	IPE160	IPE180		2,4	11	34	2664	0,973	0,817	14,167	HEA160	HEA120	HEA100	2,5	11	34	3059	0,943	0,728	13,600	HEB140	HEB100	HEB100
2,3	14	35	3203	0,949	0,920	15,217	IPE270	IPE180	IPE180		2,5	12	35	2831	0,981	0,813	14,000	HEA160	HEA120	HEA100	2,5	12	35	3217	0,939	0,778	14,000	HEB140	HEB100	HEB100
2,3	15	36	3346	0,970	0,995	15,652	IPE270	IPE180	IPE180		2,5	13	36	2966	0,969	0,880	14,400	HEA160	HEA120	HEA100	2,7	12	36	3364	0,942	0,732	13,333	HEB140	HEB100	HEB100
2,3	17	37	3706	0,951	0,974	16,087	IPE270	IPE200	IPE180		2,5	14	37	3102	0,983	0,941	14,800	HEA160	HEA120	HEA100	2,7	13	37	3530	0,930	0,789	13,704	HEB140	HEB100	HEB100
2,6	13	38	3929	0,991	0,877	14,615	IPE300	IPE180	IPE200		2,6	16	38	3365	0,968	0,948	14,615	HEA160	HEA120	HEA100	2,7	14	38	3696	0,936	0,842	14,074	HEB140	HEB100	HEB100
2,7	16	39	4170	0,953	0,925	14,444	IPE270	IPE180	IPE200		2,7	12	39	3550	0,988	0,892	14,444	HEA180	HEA120	HEA100	2,7	15	39	3862	0,940	0,905	14,444	HEB140	HEB100	HEB100
2,4	13	40	4368	0,993	0,998	16,667	IPE330	IPE200	IPE200		2,9	12	40	3695	0,984	0,840	13,793	HEA180	HEA120	HEA120	2,7	16	40	4029	0,956	0,966	14,815	HEB140	HEB100	HEB100
2,5	15	41	4603	0,978	0,947	16,400	IPE300	IPE220	IPE200		3	13	41	3913	0,964	0,849	13,667	HEA180	HEA120	HEA120	2,8	17	41	4258	0,945	0,972	14,643	HEB140	HEB100	HEB100
2,6	16	42	4849	0,964	0,944	16,154	IPE300	IPE220	IPE200		3,1	13	42	4020	0,991	0,853	13,548	HEA180	HEA120	HEA120	2,8	17	42	4669	0,984	0,971	15,000	HEB160	HEB100	HEB100
3,1	14	43	5188	0,989	0,798	13,871	IPE300	IPE200	IPE220		3,1	14	43	4201	0,991	0,903	13,871	HEA180	HEA120	HEA120	2,7	16	43	4838	0,973	0,934	15,926	HEB160	HEB120	HEB100
3	16	44	5495	0,942	0,907	14,667	IPE300	IPE200	IPE220		2,9	15	44	4483	0,939	0,961	15,172	HEA180	HEA140	HEA120	2,7	17	44	5019	0,974	0,998	16,296	HEB160	HEB120	HEB100
3,1	16	45	5644	0,972	0,907	14,516	IPE300	IPE200	IPE220		3	16	45	4717	0,921	0,960	15,000	HEA180	HEA140	HEA120	2,8	12	45	5473	0,952	0,927	16,071	HEB180	HEB120	HEB120
2,9	16	46	6041	0,921	0,945	15,862	IPE330	IPE220	IPE220		3	16	46	5074	0,939	0,964	15,333	HEA200	HEA140	HEA120	2,8	13	46	5702	0,959	0,987	16,429	HEB180	HEB120	HEB120
2,9	15	47	6328	0,973	0,958	16,207	IPE360	IPE220	IPE220		3,5	11	47	5190	0,980	0,773	13,429	HEA200	HEA140	HEA140	2,9	13	47	5849	0,971	0,981	16,207	HEB180	HEB120	HEB120
2,8	15	48	6567	0,966	0,981	17,143	IPE360	IPE240	IPE220		3,2	14	48	5574	0,937	0,951	15,000	HEA200	HEA140	HEA140	3	13	48	5996	0,984	0,975	16,000	HEB180	HEB120	HEB120
3,2	14	49	7016	0,967	0,895	15,313	IPE360	IPE220	IPE240		3,5	13	49	5669	0,941	0,859	14,000	HEA200	HEA140	HEA140	3,1	14	49	6300	0,964	0,968	15,806	HEB180	HEB120	HEB120
3,2	15	50	7296	0,970	0,950	15,625	IPE360	IPE220	IPE240		3,5	14	50	5909	0,943	0,904	14,286	HEA200	HEA140	HEA140	3,2	15	50	6615	0,952	0,972	15,625	HEB180	HEB120	HEB120
3,3	16	51	7665	0,960	0,962	15,455	IPE360	IPE220	IPE240		3,5	14	51	5984	0,979	0,950	14,571	HEA200	HEA140	HEA140	3,1	15	51	6990	0,946	0,949	16,452	HEB180	HEB140	HEB120
3,3	16	52	7991	0,951	0,912	15,758	IPE360	IPE240	IPE240		3,6	15	52	6290	0,967	0,958	14,444	HEA200	HEA140	HEA140	3,1	16	52	7241	0,946	0,998	16,774	HEB180	HEB140	HEB120
3	16	53	8571	0,940	0,985	17,667	IPE400	IPE270	IPE240		3,3	14	53	6726	0,895	0,983	16,061	HEA220	HEA160	HEA140	3,3	17	53	7655	0,913	0,948	16,061	HEB180	HEB140	HEB120
3,4	18	54	8674	0,981	0,966	15,882	IPE360	IPE240	IPE240		3,4	16	54	7196	0,889	0,988	15,882	HEA220	HEA160	HEA140	3,3	18	54	7917	0,912	0,996	16,364	HEB180	HEB140	HEB120
3,1	17	55	9406	0,955	0,954	17,742	IPE400	IPE300	IPE240		3,4	16	55	7565	0,884	0,956	16,176	HEA220	HEA180	HEA140	3,9	15	55	8458	0,992	0,888	14,103	HEB180	HEB120	HEB140
3,3	19	56	9608	0,998	0,949	16,970	IPE360	IPE300	IPE240		3,3	14	56	7791	0,962	0,993	16,970	HEA240	HEA180	HEA140	4,1	15	56	8730	0,988	0,854	13,659	HEB180	HEB120	HEB140
3,7	16	57	10029	0,953	0,920	15,405	IPE400	IPE240	IPE270		4,5	15	57	8114	0,984	0,832	12,667	HEA200	HEA140	HEA160	3,6	14	57	9072	0,936	0,924	15,833	HEB200	HEB140	HEB140
3,7	14	58	10235	0,999	0,921	15,676	IPE450	IPE240	IPE270		4,1	14	58	8400	0,929	0,853	14,146	HEA220	HEA160	HEA160	3,8	14	58	9344	0,932	0,880	15,263	HEB200	HEB140	HEB140
3,7	17	59	10816	0,977	0,922	15,946	IPE400	IPE270	IPE270		4,1	14	59	8491	0,976	0,890	14,390	HEA220	HEA160	HEA160	3,6	13	59	9613	0,994	0,978	16,389	HEB220	HEB140	HEB140
3,7	18	60	11185	0,969	0,969	16,216	IPE400	IPE270	IPE270		4,2	15	60	8902	0,932	0,900	14,286	HEA220	HEA160	HEA160	3,7	14	60	10043	0,971	0,972	16,216	HEB220	HEB140	HEB140
						15,547											13,717										14,758			

Figure B. 3: Optimized geometric variables and cross-sectional profiles for the Warren uniform IPE, HEA and HEB configuration.

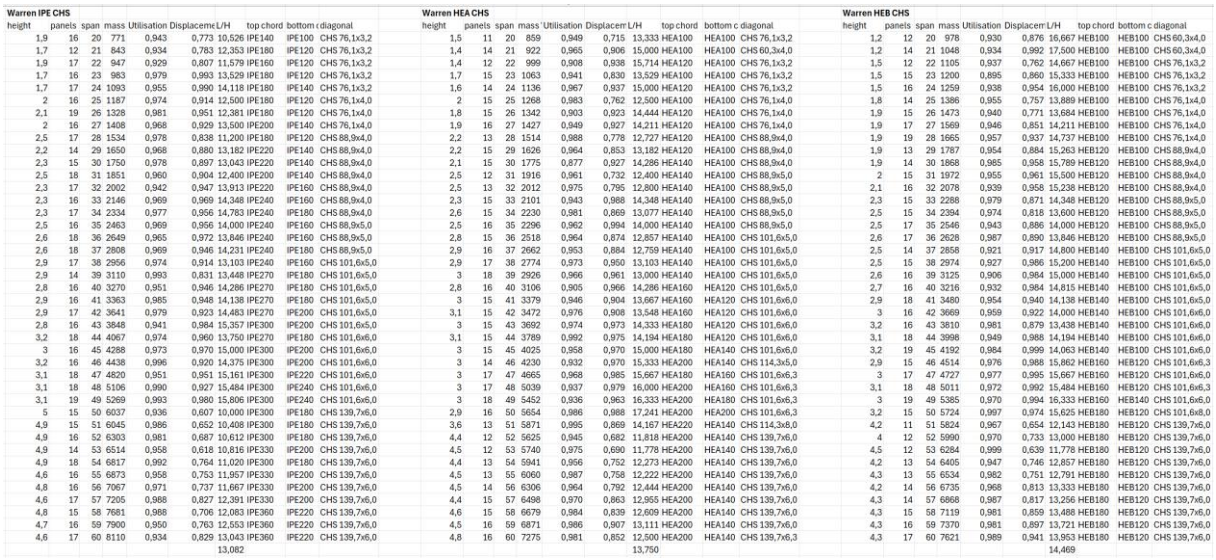

Warren IPE CHS											Warren HEA CHS										Warren HEB CHS									
height	panels	span	mass	Utilisation	Displacem	L/H	top chord	bottom c	diagonal		height	panels	span	mass	Utilisation	Displacem	L/H	top chord	bottom c	diagonal	height	panels	span	mass	Utilisation	Displacem	L/H	top chord	bottom c	diagonal	
1,9	16	20	771	0,943	0,773	10,526	IPE140	IPE100	CHS 76,1x3,2		1,5	11	20	859	0,949	0,715	13,333	HEA100	HEA100	CHS 76,1x3,2	1,2	12	20	978	0,930	0,876	16,667	HEB100	HEB100	CHS 60,3x4,0
1,7	12	21	843	0,934	0,783	12,353	IPE180	IPE120	CHS 76,1x3,2		1,4	14	21	922	0,965	0,906	15,000	HEA100	HEA100	CHS 60,3x4,0	1,2	14	21	1048	0,934	0,992	17,500	HEB100	HEB100	CHS 60,3x4,0
1,9	17	22	947	0,929	0,807	11,579	IPE160	IPE120	CHS 76,1x3,2		1,4	12	22	999	0,908	0,938	15,714	HEA120	HEA100	CHS 76,1x3,2	1,5	12	22	1105	0,937	0,762	14,667	HEB100	HEB100	CHS 76,1x3,2
1,7	16	23	983	0,979	0,993	13,529	IPE180	IPE120	CHS 76,1x3,2		1,7	15	23	1063	0,941	0,830	13,529	HEA100	HEA100	CHS 76,1x3,2	1,5	15	23	1200	0,895	0,860	15,333	HEB100	HEB100	CHS 76,1x3,2
1,7	17	24	1093	0,955	0,990	14,118	IPE180	IPE140	CHS 76,1x3,2		1,6	14	24	1136	0,967	0,937	15,000	HEA120	HEA100	CHS 76,1x3,2	1,5	16	24	1259	0,938	0,954	16,000	HEB100	HEB100	CHS 76,1x3,2
2	16	25	1187	0,974	0,914	12,500	IPE180	IPE120	CHS 76,1x4,0		2	15	25	1268	0,983	0,762	12,500	HEA100	HEA100	CHS 76,1x4,0	1,8	14	25	1386	0,955	0,757	13,889	HEB100	HEB100	CHS 76,1x4,0
2,1	19	26	1328	0,981	0,951	12,381	IPE180	IPE120	CHS 76,1x4,0		1,8	15	26	1342	0,903	0,923	14,444	HEA120	HEA100	CHS 76,1x4,0	1,9	15	26	1473	0,940	0,771	13,684	HEB100	HEB100	CHS 76,1x4,0
2	16	27	1408	0,968	0,929	13,500	IPE200	IPE140	CHS 76,1x4,0		1,9	16	27	1427	0,949	0,927	14,211	HEA120	HEA100	CHS 76,1x4,0	1,9	17	27	1569	0,946	0,851	14,211	HEB100	HEB100	CHS 76,1x4,0
2,5	17	28	1534	0,978	0,838	11,200	IPE180	IPE120	CHS 88,9x4,0		2,2	13	28	1514	0,988	0,778	12,727	HEA120	HEA100	CHS 88,9x4,0	1,9	19	28	1665	0,957	0,937	14,737	HEB100	HEB100	CHS 76,1x4,0
2,2	14	29	1650	0,968	0,880	13,182	IPE220	IPE140	CHS 88,9x4,0		2,2	15	29	1626	0,964	0,853	13,182	HEA120	HEA100	CHS 88,9x4,0	1,9	13	29	1787	0,954	0,884	15,263	HEB120	HEB100	CHS 88,9x4,0
2,3	15	30	1750	0,978	0,897	13,043	IPE220	IPE140	CHS 88,9x4,0		2,1	15	30	1775	0,877	0,927	14,286	HEA140	HEA100	CHS 88,9x4,0	1,9	14	30	1868	0,985	0,958	15,789	HEB120	HEB100	CHS 88,9x4,0
2,5	18	31	1851	0,960	0,904	12,400	IPE200	IPE140	CHS 88,9x4,0		2,5	12	31	1916	0,961	0,732	12,400	HEA140	HEA100	CHS 88,9x5,0	2	15	31	1972	0,955	0,961	15,500	HEB120	HEB100	CHS 88,9x4,0
2,3	17	32	2002	0,942	0,947	13,913	IPE220	IPE160	CHS 88,9x4,0		2,5	13	32	2012	0,975	0,795	12,800	HEA140	HEA100	CHS 88,9x5,0	2,1	16	32	2078	0,939	0,958	15,238	HEB120	HEB100	CHS 88,9x4,0
2,3	16	33	2146	0,969	0,969	14,348	IPE240	IPE160	CHS 88,9x4,0		2,3	15	33	2101	0,943	0,988	14,348	HEA140	HEA100	CHS 88,9x5,0	2,3	15	33	2288	0,979	0,871	14,348	HEB120	HEB100	CHS 88,9x5,0
2,3	17	34	2334	0,977	0,956	14,783	IPE240	IPE180	CHS 88,9x4,0		2,6	15	34	2230	0,981	0,869	13,077	HEA140	HEA100	CHS 88,9x5,0	2,5	15	34	2394	0,974	0,818	13,600	HEB120	HEB100	CHS 88,9x5,0
2,5	16	35	2463	0,969	0,956	14,000	IPE240	IPE160	CHS 88,9x5,0		2,5	16	35	2296	0,962	0,994	14,000	HEA140	HEA100	CHS 88,9x5,0	2,5	17	35	2546	0,943	0,886	14,000	HEB120	HEB100	CHS 88,9x5,0
2,6	18	36	2649	0,965	0,972	13,846	IPE240	IPE160	CHS 88,9x5,0		2,8	15	36	2518	0,964	0,874	12,857	HEA140	HEA100	CHS 101,6x5,0	2,6	17	36	2628	0,987	0,890	13,846	HEB120	HEB100	CHS 88,9x5,0
2,6	18	37	2808	0,969	0,946	14,231	IPE240	IPE180	CHS 88,9x5,0		2,9	16	37	2662	0,953	0,884	12,759	HEA140	HEA100	CHS 101,6x5,0	2,5	14	37	2858	0,921	0,917	14,800	HEB140	HEB100	CHS 101,6x5,0
2,9	17	38	2956	0,974	0,914	13,103	IPE240	IPE160	CHS 101,6x5,0		2,9	17	38	2774	0,973	0,950	13,103	HEA140	HEA100	CHS 101,6x5,0	2,5	15	38	2974	0,927	0,986	15,200	HEB140	HEB100	CHS 101,6x5,0
2,9	14	39	3110	0,993	0,831	13,448	IPE270	IPE180	CHS 101,6x5,0		3	18	39	2926	0,966	0,961	13,000	HEA140	HEA100	CHS 101,6x5,0	2,6	16	39	3125	0,906	0,984	15,000	HEB140	HEB100	CHS 101,6x5,0
2,8	16	40	3270	0,951	0,946	14,286	IPE270	IPE180	CHS 101,6x5,0		2,8	16	40	3106	0,905	0,966	14,286	HEA160	HEA120	CHS 101,6x5,0	2,7	16	40	3216	0,932	0,984	14,815	HEB140	HEB100	CHS 101,6x5,0
2,9	16	41	3363	0,985	0,948	14,138	IPE270	IPE180	CHS 101,6x5,0		3	15	41	3379	0,946	0,904	13,667	HEA160	HEA120	CHS 101,6x6,0	2,9	18	41	3480	0,954	0,940	14,138	HEB140	HEB100	CHS 101,6x5,0
2,9	17	42	3641	0,979	0,923	14,483	IPE270	IPE200	CHS 101,6x5,0		3,1	15	42	3472	0,976	0,908	13,548	HEA160	HEA120	CHS 101,6x6,0	3	16	42	3669	0,959	0,922	14,000	HEB140	HEB100	CHS 101,6x6,0
2,8	16	43	3848	0,941	0,984	15,357	IPE300	IPE200	CHS 101,6x5,0		3	15	43	3692	0,974	0,973	14,333	HEA180	HEA120	CHS 101,6x6,0	3,2	16	43	3810	0,981	0,879	13,438	HEB140	HEB100	CHS 101,6x6,0
3,2	18	44	4067	0,974	0,960	13,750	IPE270	IPE180	CHS 101,6x6,0		3,1	15	44	3789	0,992	0,975	14,194	HEA180	HEA120	CHS 101,6x6,0	3,1	18	44	3998	0,949	0,988	14,194	HEB140	HEB100	CHS 101,6x6,0
3	16	45	4288	0,973	0,970	15,000	IPE300	IPE200	CHS 101,6x6,0		3	15	45	4025	0,958	0,970	15,000	HEA180	HEA140	CHS 101,6x6,0	3,2	19	45	4192	0,984	0,999	14,063	HEB140	HEB100	CHS 101,6x6,0
3,2	16	46	4438	0,996	0,920	14,375	IPE300	IPE200	CHS 101,6x6,0		3	14	46	4230	0,932	0,970	15,333	HEA200	HEA140	CHS 114,3x5,0	2,9	15	46	4514	0,976	0,988	15,862	HEB160	HEB120	CHS 101,6x6,3
3,1	18	47	4820	0,951	0,951	15,161	IPE300	IPE220	CHS 101,6x6,0		3	17	47	4665	0,968	0,985	15,667	HEA180	HEA160	CHS 101,6x6,3	3	17	47	4727	0,977	0,995	15,667	HEB160	HEB120	CHS 101,6x6,0
3,1	18	48	5106	0,990	0,927	15,484	IPE300	IPE240	CHS 101,6x6,0		3	17	48	5039	0,937	0,979	16,000	HEA200	HEA160	CHS 101,6x6,3	3,1	18	48	5011	0,972	0,992	15,484	HEB160	HEB120	CHS 101,6x6,3
3,1	19	49	5269	0,993	0,980	15,806	IPE300	IPE240	CHS 101,6x6,0		3	18	49	5452	0,936	0,963	16,333	HEA200	HEA180	CHS 101,6x6,3	3	19	49	5385	0,970	0,994	16,333	HEB160	HEB140	CHS 101,6x6,0
5	15	50	6037	0,936	0,607	10,000	IPE300	IPE180	CHS 139,7x6,0		2,9	16	50	5654	0,986	0,988	17,241	HEA200	HEA200	CHS 101,6x6,3	3,2	15	50	5724	0,997	0,974	15,625	HEB180	HEB120	CHS 101,6x8,0
4,9	15	51	6045	0,986	0,652	10,408	IPE300	IPE180	CHS 139,7x6,0		3,6	13	51	5871	0,995	0,869	14,167	HEA220	HEA140	CHS 114,3x8,0	4,2	11	51	5824	0,967	0,654	12,143	HEB180	HEB120	CHS 139,7x6,0
4,9	16	52	6303	0,981	0,687	10,612	IPE300	IPE180	CHS 139,7x6,0		4,4	12	52	5625	0,945	0,682	11,818	HEA200	HEA140	CHS 139,7x6,0	4	12	52	5990	0,970	0,733	13,000	HEB180	HEB120	CHS 139,7x6,0
4,9	14	53	6514	0,958	0,618	10,816	IPE330	IPE200	CHS 139,7x6,0		4,5	12	53	5740	0,975	0,690	11,778	HEA200	HEA140	CHS 139,7x6,0	4,5	12	53	6284	0,999	0,639	11,778	HEB180	HEB120	CHS 139,7x6,0
4,9	18	54	6817	0,992	0,764	11,020	IPE300	IPE180	CHS 139,7x6,0		4,4	13	54	5941	0,956	0,752	12,273	HEA200	HEA140	CHS 139,7x6,0	4,2	13	54	6405	0,947	0,746	12,857	HEB180	HEB120	CHS 139,7x6,0
4,6	16	55	6873	0,958	0,753	11,957	IPE330	IPE200	CHS 139,7x6,0		4,5	13	55	6060	0,987	0,758	12,222	HEA200	HEA140	CHS 139,7x6,0	4,3	13	55	6534	0,982	0,751	12,791	HEB180	HEB120	CHS 139,7x6,0
4,8	16	56	7067	0,971	0,737	11,667	IPE330	IPE200	CHS 139,7x6,0		4,5	14	56	6306	0,964	0,792	12,444	HEA200	HEA140	CHS 139,7x6,0	4,2	14	56	6735	0,968	0,813	13,333	HEB180	HEB120	CHS 139,7x6,0
4,6	17	57	7205	0,988	0,827	12,391	IPE330	IPE200	CHS 139,7x6,0		4,4	15	57	6498	0,970	0,863	12,955	HEA200	HEA140	CHS 139,7x6,0	4,3	14	57	6868	0,987	0,817	13,256	HEB180	HEB120	CHS 139,7x6,0
4,8	15	58	7681	0,988	0,706	12,083	IPE360	IPE220	CHS 139,7x6,0		4,6	15	58	6679	0,984	0,839	12,609	HEA200	HEA140	CHS 139,7x6,0	4,3	15	58	7119	0,981	0,859	13,488	HEB180	HEB120	CHS 139,7x6,0
4,7	16	59	7900	0,950	0,763	12,553	IPE360	IPE220	CHS 139,7x6,0		4,5	16	59	6871	0,986	0,907	13,111	HEA200	HEA140	CHS 139,7x6,0	4,3	16	59	7370	0,981	0,897	13,721	HEB180	HEB120	CHS 139,7x6,0
4,6	17	60	8110	0,934	0,829	13,043	IPE360	IPE220	CHS 139,7x6,0		4,8	16	60	7275	0,981	0,852	12,500	HEA200	HEA140	CHS 139,7x6,3	4,3	17	60	7621	0,989	0,941	13,953	HEB180	HEB120	CHS 139,7x6,0
						13,082											13,750										14,469			

Figure B. 4: Optimized geometric variables and cross-sectional profiles for the Warren uniform IPE CHS, HEA CHS and HEB CHS configuration.

B.3 Parker

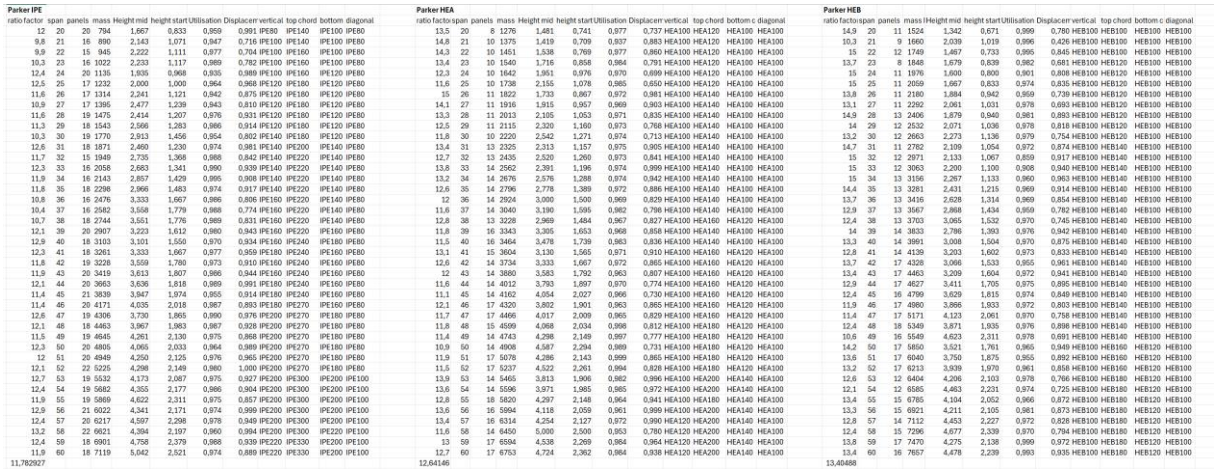

| Parker IPE | | |

Appendix C: Additional mass efficiency data

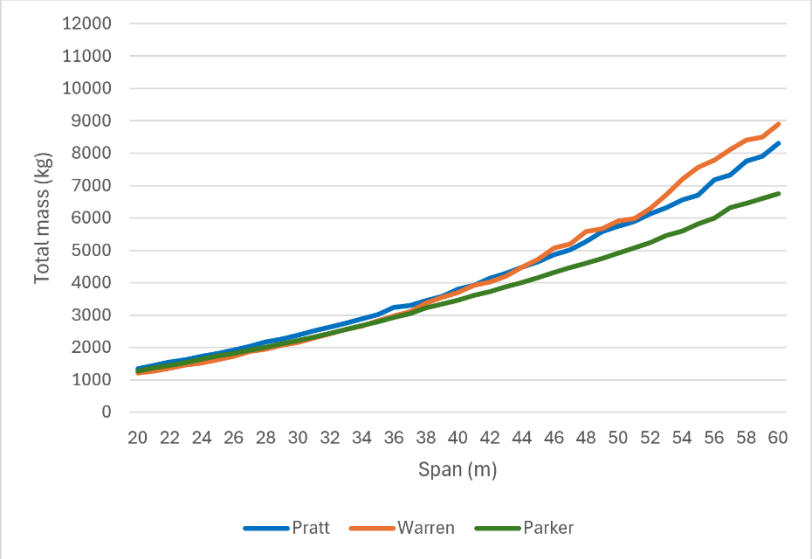

Figure C. 1: Total structural mass of the Pratt, Warren, and Parker topologies across a 20 to 60-meter span, utilizing uniform HEA cross-sections (Dataset 2).

Appendix D: Uniform versus hybrid configurations

D.1 Pratt

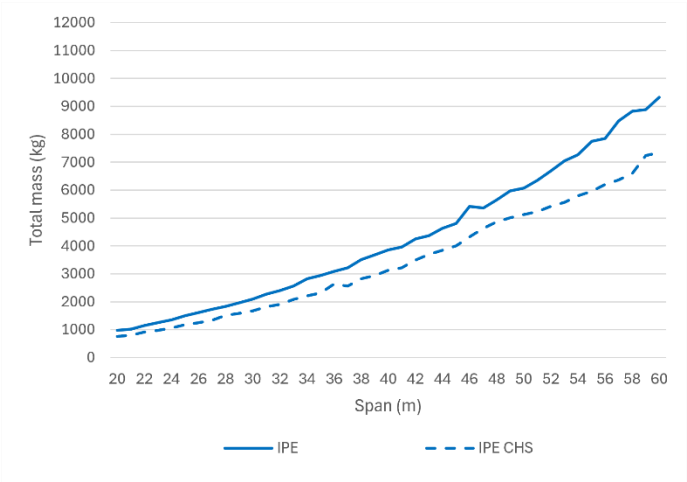

Figure D. 1: Total mass of the uniform IPE versus the hybrid IPE CHS configuration for the Pratt truss.

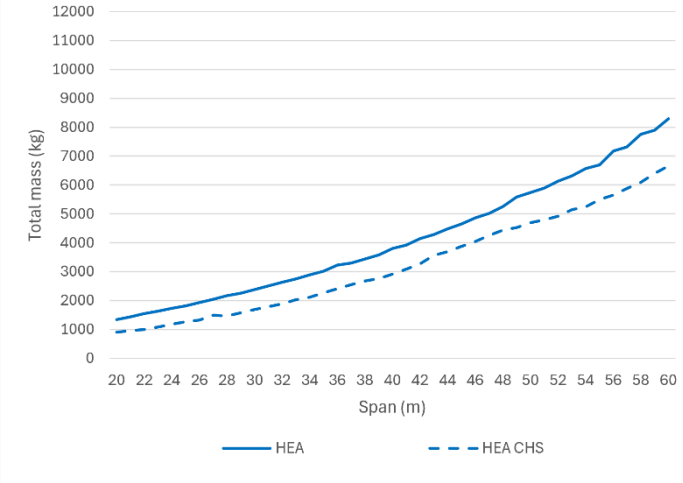

Figure D. 2: Total mass of the uniform HEA versus the hybrid HEA CHS configuration for the Pratt truss.

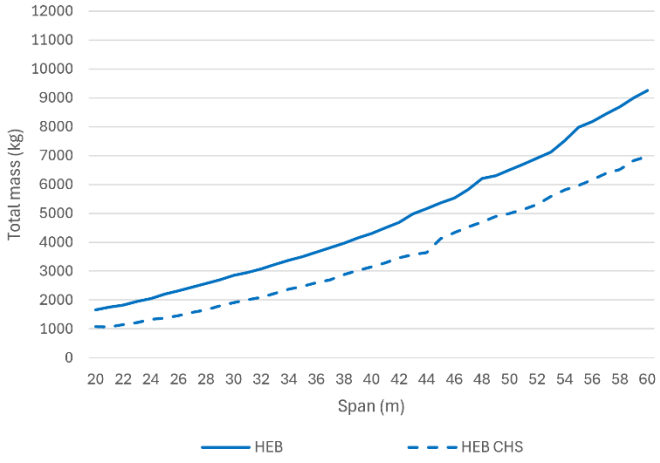

Figure D. 3: Total mass of the uniform HEB versus the hybrid HEB CHS configuration for the Pratt truss.

D.2 Warren

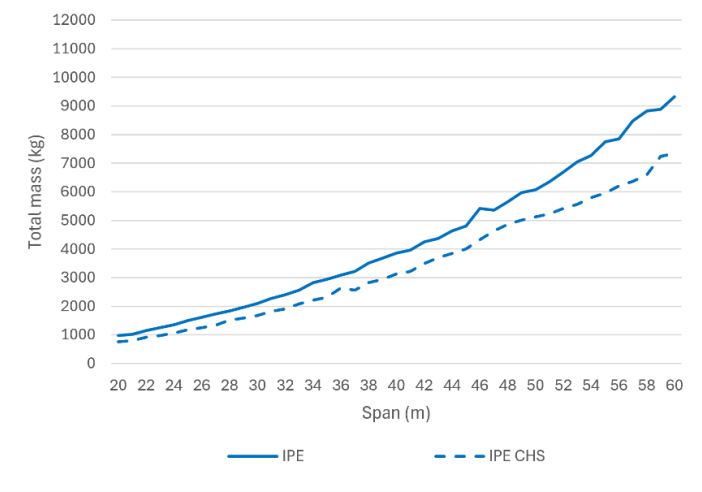

Figure D. 4: Total mass of the uniform IPE versus the hybrid IPE CHS configuration for the Warren truss.

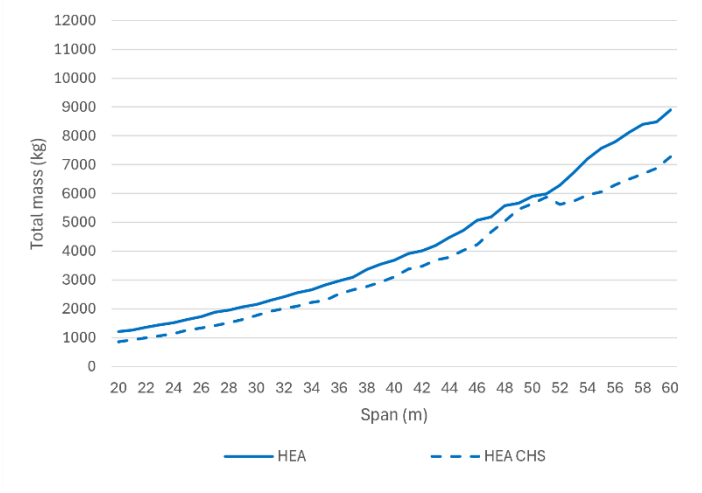

Figure D. 5: Total mass of the uniform HEA versus the hybrid HEA CHS configuration for the Warren truss.

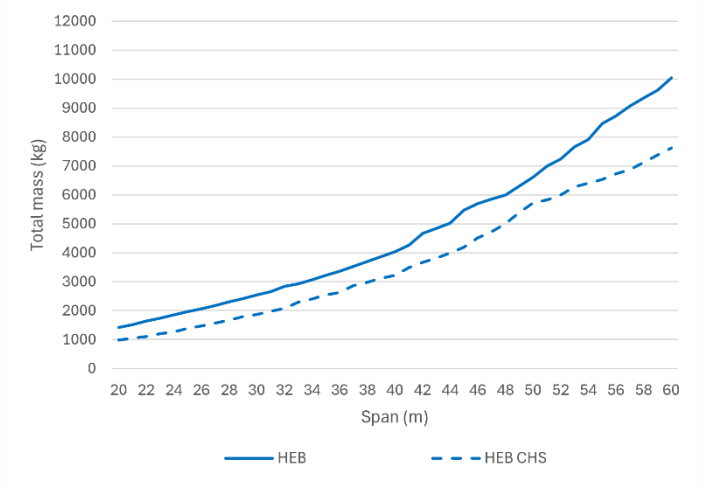

Figure D. 6: Total mass of the uniform HEB versus the hybrid HEB CHS configuration for the Warren truss.

D.3 Parker

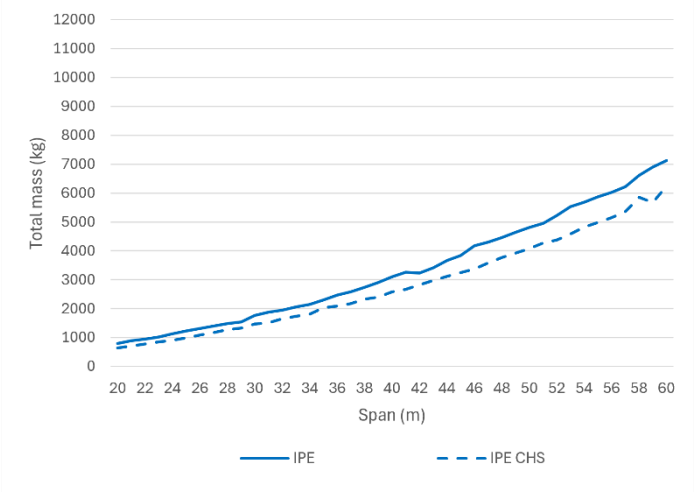

Figure D. 7: Total mass of the uniform IPE versus the hybrid IPE CHS configuration for the Parker truss.

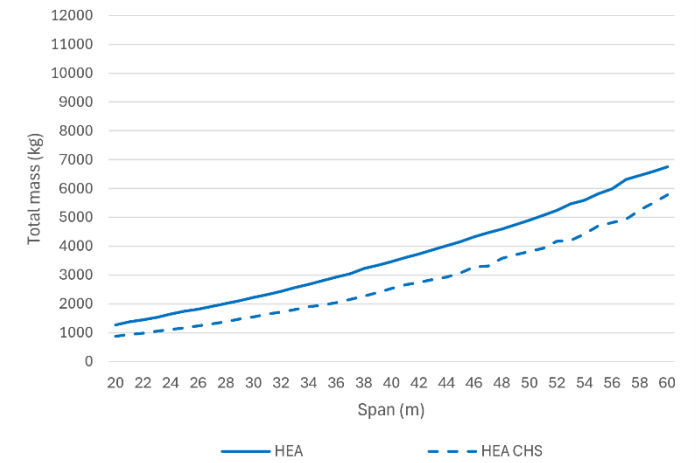

Figure D. 8: Total mass of the uniform HEA versus the hybrid HEA CHS configuration for the Parker truss.

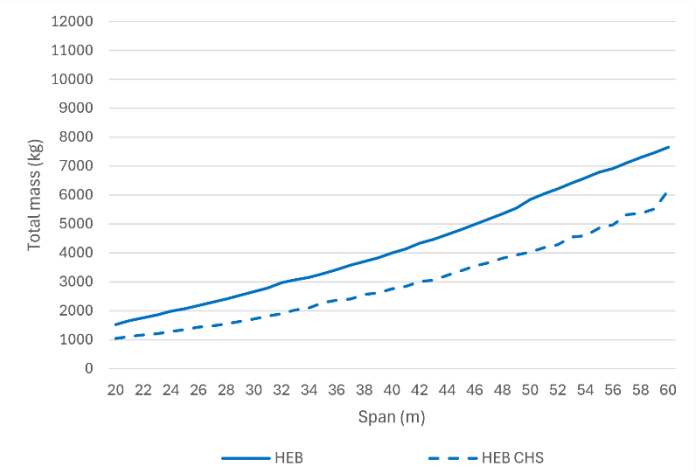

Figure D. 9: Total mass of the uniform HEB versus the hybrid HEB CHS configuration for the Parker truss.

Appendix E: Span-to-height ratios for HEA and HEB

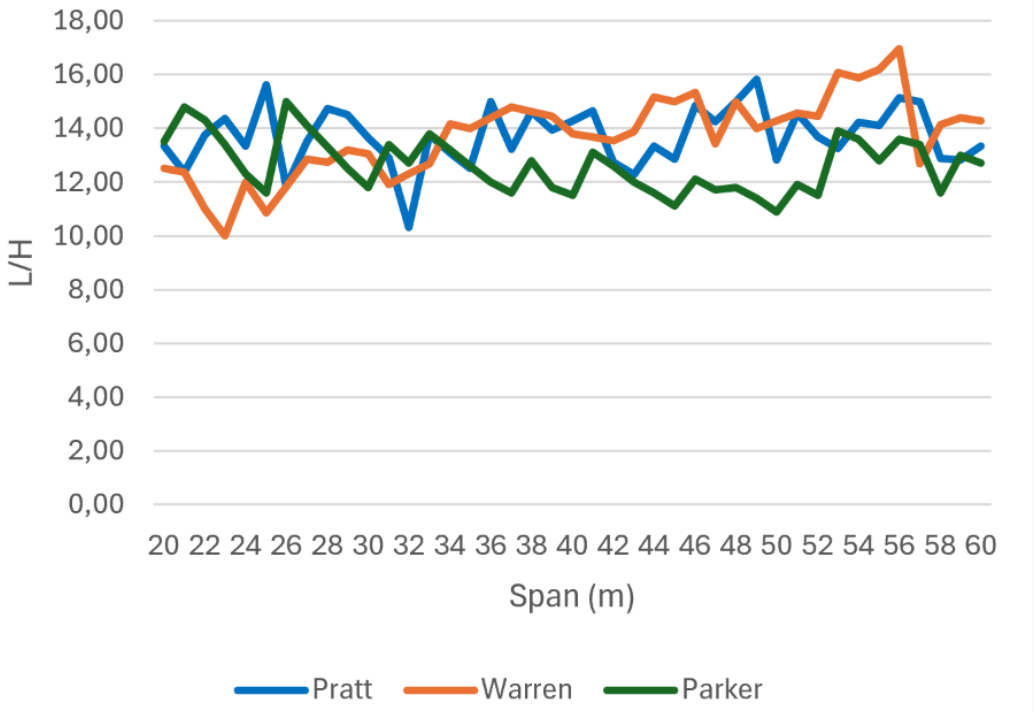

Figure E. 1: Optimal span-to-height (L/H) ratios for the Pratt, Warren and Parker topologies across the 20 to 60-meter span range, based on the HEA datasets.

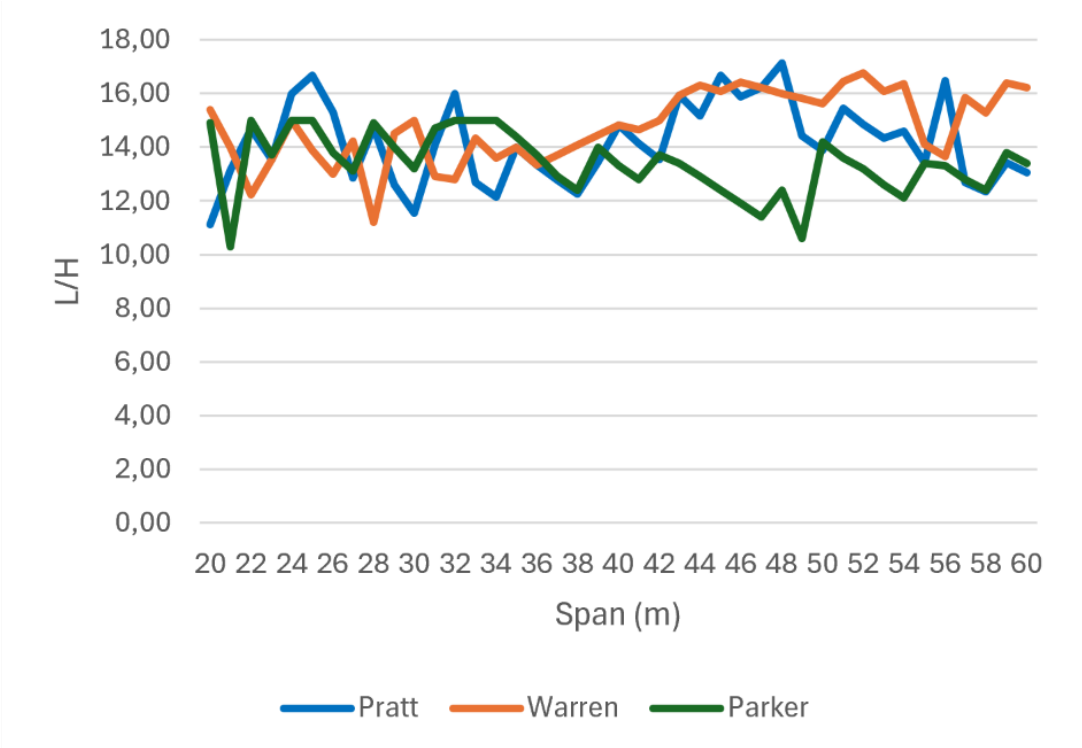

Figure E. 2: Optimal span-to-height (L/H) ratios for the Pratt, Warren and Parker topologies across the 20 to 60-meter span range, based on the HEB datasets.

Appendix F: ULS versus SLS

F.1 IPE

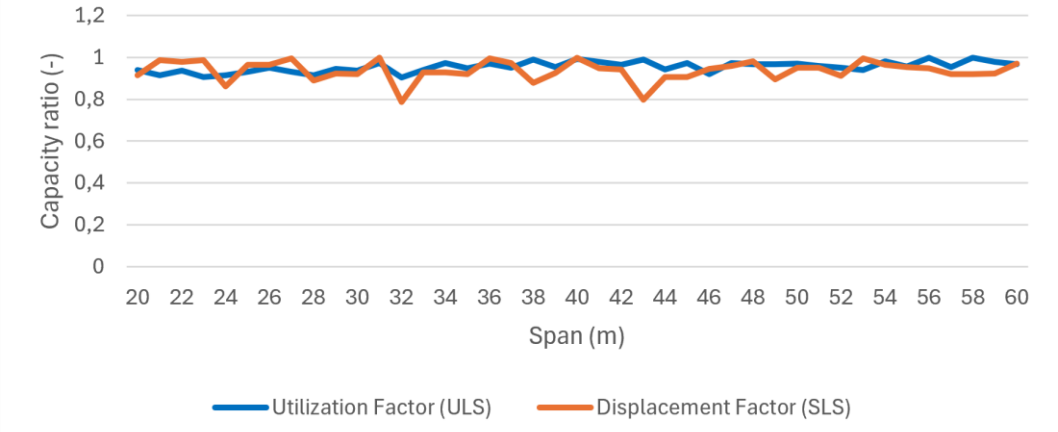

Figure F. 1: Cross-section utilization (ULS) versus vertical displacement (SLS) across the evaluated span range for the Warren topology (IPE dataset).

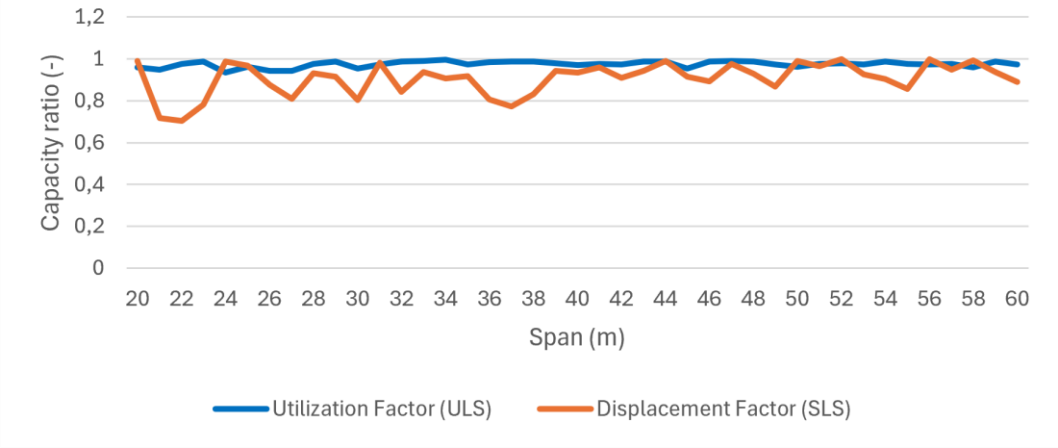

Figure F. 2: Cross-section utilization (ULS) versus vertical displacement (SLS) across the evaluated span range for the Parker topology (IPE dataset).

F.2 HEA

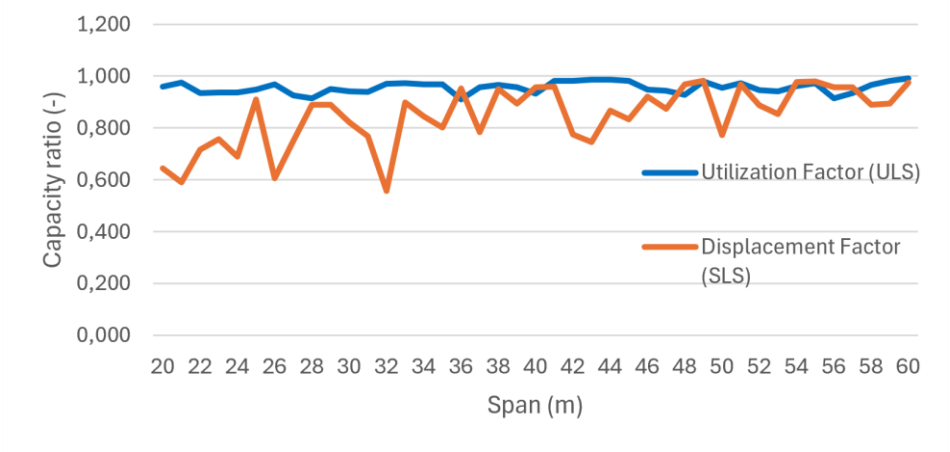

Figure F. 3: Cross-section utilization (ULS) versus vertical displacement (SLS) across the evaluated span range for the Pratt topology (HEA dataset).

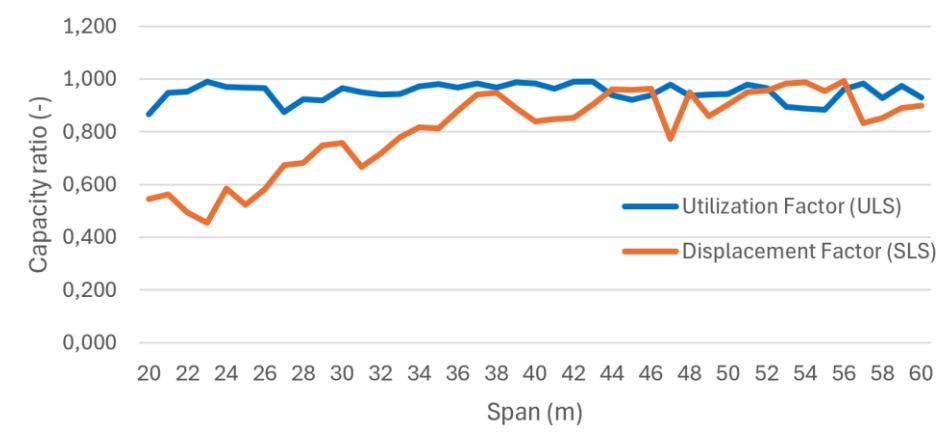

Figure F. 4: Cross-section utilization (ULS) versus vertical displacement (SLS) across the evaluated span range for the Warren topology (HEA dataset).

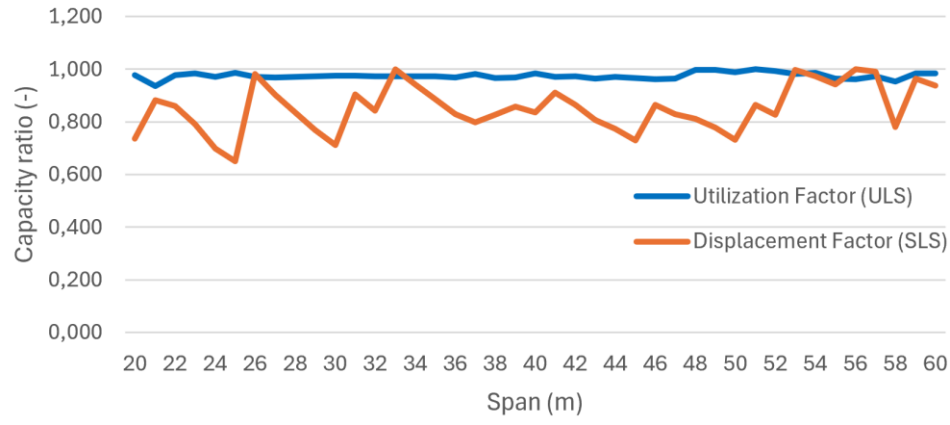

Figure F. 5: Cross-section utilization (ULS) versus vertical displacement (SLS) across the evaluated span range for the Parker topology (HEA dataset).

F.3 HEB

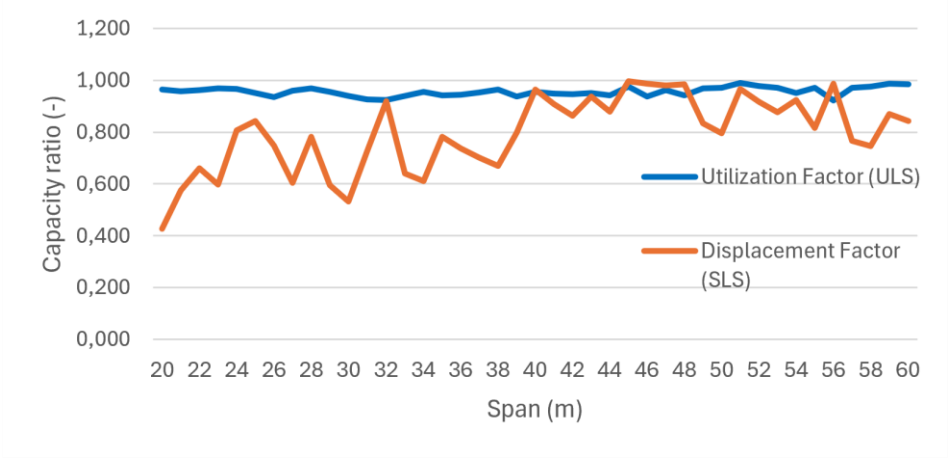

Figure F. 6: Cross-section utilization (ULS) versus vertical displacement (SLS) across the evaluated span range for the Pratt topology (HEB dataset).

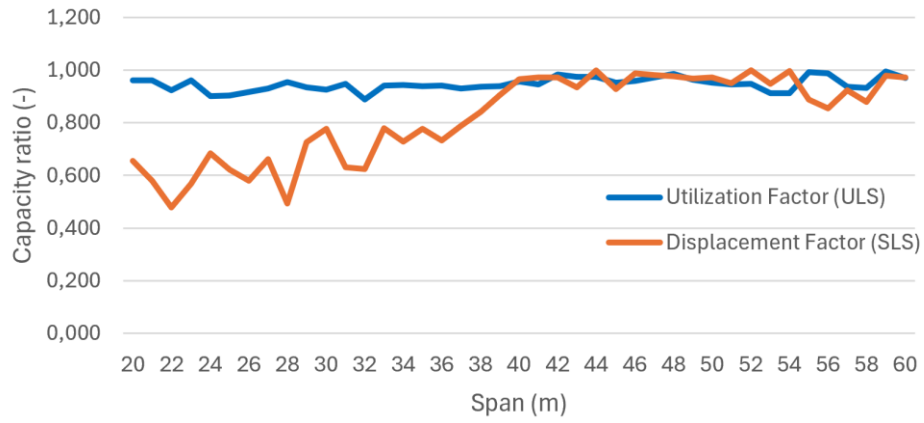

Figure F. 7: Cross-section utilization (ULS) versus vertical displacement (SLS) across the evaluated span range for the Warren topology (HEB dataset).

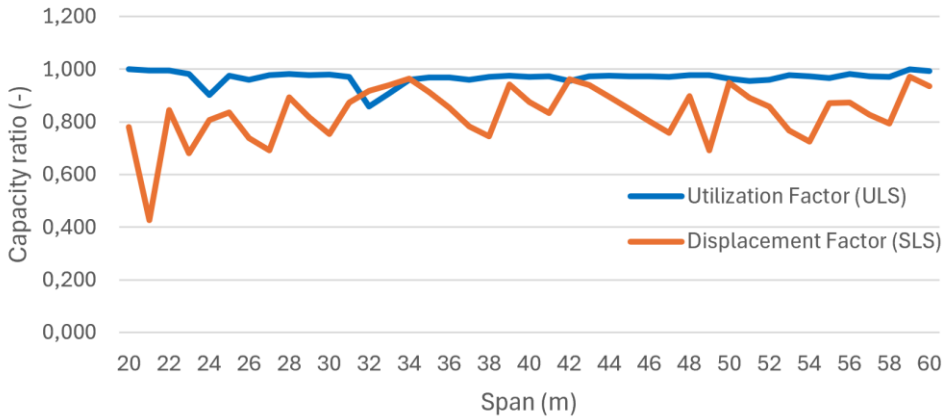

Figure F. 8: Cross-section utilization (ULS) versus vertical displacement (SLS) across the evaluated span range for the Parker topology (HEB dataset).

References

Andersson, V., & Hillberg, C. (2018). *Evolutionary optimization of steel truss footbridges: A study of parametric design and optimization in Karamba 3D, Galapagos and Octopus for different truss geometries (Master's thesis ACEX30-18-35)* (Publication Number Master's thesis ACEX30-18-35) Chalmers University of Technology].

Barker, R. M., & Puckett, J. A. (2013). *Design of Highway Bridges: An LRFD Approach*. John Wiley & Sons.

Hibbeler, R. C. (2012). *Structural Analysis*. Prentice Hall.

Kostić, N., Petrović, N., Marjanović, V., Nikolić, R. R., Szmidla, J., Marjanović, N., & Ulewicz, R. (2024). Effects of Limiting the Number of Different Cross-Sections Used in Statically Loaded Truss Sizing and Shape Optimization. *Materials*, *17*(6), 1390. https://doi.org/10.3390/ma17061390

Kulicki, J. M. (2014). Highway Truss Bridges. In W.-F. D. Chen, Lian (Ed.), *Bridge Engineering Handbook: Superstructure Design* (2nd ed. ed.). CRC Press.

Kumar, S. S., & Kumar, A. S. (2018). *Design of Steel Structures: Truss Bridges*. Indian Institute of Technology Madras (IITM).

Li, P., Zhao, X., Ding, D., Li, X., Zhao, Y., Ke, L., Zhang, X., & Jian, B. (2023). Optimization Design for Steel Trusses Based on a Genetic Algorithm. *Buildings*, *13*(6), 1496. https://doi.org/10.3390/buildings13061496

Nadimalla, A. K., & Vanakudre, S. B. (2012). ANALYSIS AND DESIGN OF STEEL TRUSSES BY POST-TENSIONING METHOD USING SAP2000v15. *Global Journal of Engineering & Applied Sciences*, *2*(2), 220-224.

National Steel Bridge Alliance (NSBA). (2025). Selecting the Right Bridge Type. In *Steel Bridge Design Handbook*. American Institute of Steel Construction (AISC).

NEN-EN 1990-1:2025+A1:2026. Eurocode - Grondslagen van het constructief en geotechnisch ontwerp - Deel 1: Nieuwe constructies. In (Vol. NEN-EN 1990-1:2025+A1:2026 en): Nederlands Normalisatie-instituut,.

NEN-EN 1991-2:2025. Eurocode 1 - Actions on structures - Part 2: Traffic

loads on bridges and other civil engineering

works. In: Nederlands Normalisatie-instituut (NEN).

NEN-EN 1993-1-1. Eurocode 3: Design of steel structures - Part 1-1: General rules and rules for buildings. In: Nederlands Normalisatie-instituut (NEN).

Nguyen, Q. B., Nguyen, H.-H., & Ha, M.-H. (2024). An Efficient Framework for Optimization of Nonlinear Steel Trusses with Continuous Variables. *International Journal of GEOMATE*, *25*.

Roughan & O'Donovan Consulting Engineers. (2025). *N59 Oughterard Footbridge: Structure Options Report*.

Wardenier, J., Packer, J. A., Zhao, X. L., & van der Vegte, G. J. (2010). *Hollow Sections in Structural Applications* (2nd ed.). CIDECT / Bouwen met Staal.

Yavan, F., Maalek, R., & Toğan, V. (2024). Structural Optimization of Trusses Using Visual Programming and Evolutionary Algorithms. *Buildings*, *14*(6), 1532.